

# Scattering of magnetostatic surface modes of ferromagnetic films by geometric defects

R. E. Arias *Departamento de Física, CEDENNA, Facultad de Ciencias Físicas y Matemáticas, Universidad de Chile, Santiago 8370456, Chile*

(Received 15 May 2023; revised 11 October 2023; accepted 24 October 2023; published 6 November 2023)

Magnonics, an emerging field of magnetism, studies spin waves (SWs) in nanostructures, with an aim towards possible applications. As information may be eventually transmitted with efficiency stored in the phase and amplitude of spin waves, a topic of interest within magnonics is the propagation of SW modes. Thus understanding mechanisms that may influence SW propagation is of interest. Here the effect of localized surface geometric defects on magnetostatic surface modes propagation is studied in ferromagnetic films and semi-infinite media. Theoretical results are developed that allow one to calculate the scattering of these surface or Damon-Eshbach (DE) modes. A Green's-extinction theorem extension is used to determine the scattering of incident surface modes through the determination of phase shifts of associated modes that are symmetric and antisymmetric under inversion in the same geometry with geometric defects. Choosing localized symmetric depressions as geometric defects, scattering transmission coefficients are determined that show perfect transmission at specific frequencies or wavelengths that we associate with resonances in the system: they do occur when appropriate fractions of the incoming wavelength "fit" with the approximate depression's sizes, i.e., depressions are effectively similar to "potential wells." Interestingly the system also shows the appearance of localized modes in the depression regions, with associated discrete frequencies immersed in the continuum spectrum of these surface DE modes. These localized modes have a short wavelength content and appear similarly in semi-infinite surfaces with depressions. The latter indicates that these types of scattering effects should appear in all surfaces with roughness or more pronounced geometric defects.

DOI: [10.1103/PhysRevB.108.174408](https://doi.org/10.1103/PhysRevB.108.174408)

## I. INTRODUCTION

A present area of interest, that has been developed mainly in the past couple of decades, is magnonics [1,2], which studies spin waves in nanostructures [3,4] with an aim towards possible technological applications [5–7]. Among the advantages of spin waves to transmit information are low consumption of energy, long transmission lengths, and operation at microwave frequencies with wavelengths at the nanoscale, i.e., compatible with nanocircuits. Within magnonics a particular topic of interest is propagation of spin waves in waveguides, since the control of proper transmission of information coded either in the amplitude or phase of a spin wave is crucial for applications. The present study corresponds to the latter topic of interest, since it delves with the effect of geometric defects on the propagation of magnetostatic surface waves or Damon-Eshbach (DE) [8] waves. In particular we study, as an example of localized geometric defects, the effect of depressions in the scattering of DE modes in ferromagnetic thin films and semi-infinite media.

Magnetostatic surface or volume modes have been studied in ferromagnetic films for a long time since the 1950s and even up to the present, in different ways. One may mention theoretical studies [9,10] and experimental ones [11–13] that have dealt with these modes in ferromagnetic films. Surface magnetostatic modes have the advantage that they may propagate long distances, in the order of several microns [12,14], they may have large group velocities, and they do not require large applied magnetic fields.

The scattering of spin waves by different types of defects/inhomogeneities/textures in films and waveguides

has been studied theoretically and experimentally. A few of these types of studies are scattering by regions of inhomogeneous magnetic fields [15,16], by a localized defect [17], by nanodefects and nanowells [18,19], by one dimensional steps [20], and by magnetic textures as skyrmions and domain walls [21–26].

The surface geometric defects considered in the present theoretical study correspond to effectively two-dimensional (2D) geometric features [no variation along a transverse direction ( $z$ )] that do not alter the equilibrium magnetization of this Damon-Eshbach geometry: there is an in plane applied magnetic field with which the equilibrium magnetization aligns itself and the surface spin waves propagate perpendicular to this latter direction. The scattering of the magnetostatic surface waves is analyzed in these films using an extension of the Green's-extinction theorem [39] method: it has been used by the author and co-workers in previous works, either in the magnetostatic approximation [27–29] (the latter reference studied periodic surface geometric defects, with an associated appearance of frequency band gaps) or in the dipole-exchange approximation [30–32]. The latter studies introduced "auxiliary functions" as part of the Green's-extinction method, an approach that is also used in the present study and that was named there the "orthogonal equations" method [32]. The mentioned method allows one to write integral equations for the spin wave modes evaluated on the surfaces (these may have arbitrary shapes in principle) and their corresponding eigenfrequencies. Indeed, after the integral equations are solved on the surface of the sample one may obtain the shape of the modes everywhere in space, if desired.

The theoretical analysis of the magnetostatic scattering results has many similarities with a simpler case study that has been well researched and where a great deal of analytical progress has been possible: this corresponds to 1D scattering of a quantum mechanical particle by a localized potential. The associated Schrödinger equation has been well studied and scattering theories developed [33–37].

An analysis of the flow of energy [10,38] in the scattering process of a surface magnetostatic wave by surface geometric defects allows one to determine reflection and transmission coefficients. Also, an analysis in terms of the orthogonal equations method [32] allows one to determine the phase shifts of eigenmode solutions that are “symmetric” and “antisymmetric” under inversion in the presence of these geometric defects. As well as in the simpler 1D quantum particles scattering [33,34], the scattering solution of an incident magnetostatic surface wave may be related with these symmetric and antisymmetric modes and indeed the reflection and transmission coefficients may be directly written in terms of the difference between the previously mentioned phase shifts.

Results are presented that apply the previous theory to an example of geometric defects: depressions symmetrically located on both surfaces of the film. The transmission coefficient as function of frequency or incident wavelength presents resonances associated with perfect transmission and also interestingly some localized modes appear at the location of the defects: the latter start appearing at short wavelengths and they are also present with basically the same features in a semi-infinite medium.

## II. MAGNETIZATION DYNAMICS

### A. Samples and magnetostatic surface modes configuration

We study scattering of magnetostatic surface modes in ferromagnetic films and semi-infinite media with geometric defects localized at the surfaces. We assume these defects to be geometric perturbations invariant in the  $z$  direction and that there is a magnetic field applied in this direction,  $\vec{H}_{app} = H_0\hat{z}$ : this determines that there is a uniform equilibrium magnetization,  $M_s\hat{z}$ , parallel to the applied magnetic field. We consider wave propagation in the  $\pm\hat{x}$  directions with invariance along the transverse  $z$  direction. Thus the fields associated to the wave propagation vary effectively in two dimensions, the  $x - y$  plane, with  $y$  the direction perpendicular to the surfaces of the film or the semi-infinite medium. This geometry, magnetic field, and wave propagation directions correspond to the so called Damon-Eshbach (DE) configuration [8], i.e., propagation perpendicular to the equilibrium magnetization, where it is well known that magnetostatic surface modes propagate [8].

The perfect or unperturbed geometries that we consider correspond to ferromagnetic films of thickness  $w = 2l$  (surfaces at  $y = \pm l$ ) or a semi-infinite ferromagnetic medium at  $y \geq 0$ . Given the applied magnetic field direction, in a semi-infinite medium these modes propagate only in one direction at frequency  $\omega = |\gamma|(H_0 + 2\pi M_s)$  (in our case in the  $\hat{x}$  direction;  $\gamma$  is the gyromagnetic factor and  $M_s$  the saturation magnetization). In a ferromagnetic film Damon-Eshbach surface modes propagating in different directions are

reciprocal in frequencies but nonreciprocal in shape [8]: a right propagating mode ( $\hat{x}$  direction) has its main amplitude associated with the lower surface of the film ( $y = -l$ ), while a left propagating mode has amplitude mainly in the opposite upper surface. The dispersion relation of the magnetostatic DE modes is known analytically as [8]

$$\Omega = \sqrt{(h_0 + 1/2)^2 - e^{-4|k|l}/4}, \quad (1)$$

where  $\Omega \equiv \omega/4\pi M_s|\gamma|$  represents normalized frequencies,  $h_0 \equiv H_0/4\pi M_s$  a nondimensional magnitude of the applied magnetic field, and  $k$  the wave vector of the surface modes. Thus the lower end frequencies of this dispersion relation correspond to the long wavelength DE modes that have frequencies starting at  $\Omega = \sqrt{h_0(h_0 + 1)}$  (which is the upper limit of the bulk modes) and the upper frequencies limit corresponds to the short wavelength surface modes that have frequencies that end at  $\Omega = h_0 + 1/2$ , i.e., at the mentioned frequency of surface waves in a semi-infinite medium. One may say that the finite thickness  $w = 2l$  of the film, or effectively the presence of two opposing surfaces, has opened up the degeneracy of the surface modes of a semi-infinite medium at the frequency  $\Omega = h_0 + 1/2$ . Indeed, the long wavelength surface modes change their frequencies the most; this may be understood since the amplitude of the surface modes penetrates a distance of the order of their wavelength  $\lambda$  into the medium, i.e., the long wavelength modes “feel the effect” of the other surface of the film when  $\lambda \sim l$ , which is reflected in the dispersion relation of Eq. (1).

The geometric defects that we consider alter the surfaces of the semi-infinite medium and the film, such that their new surfaces are described as  $y = \xi(x)$  for the first and as  $y = l + \eta(x)$  for the upper surface of the film and  $y = -l + \xi(x)$  for the lower. We consider these defects to be localized perturbations, i.e., the geometries are flat at  $x \rightarrow \pm\infty$ , and that they are even with respect to  $x = 0$  (this allows one to simplify the analysis of the scattering problem in terms of spin wave modes with symmetry properties). Given these defects, the equilibrium magnetization is unaltered; it continues to be uniform and parallel to the geometric defects’ directions since these defects do not induce effective magnetic charges for  $M_s\hat{z}$ . The magnetostatic approximation used here should be valid for wavelengths larger than the exchange length of the ferromagnet. Thus one expects this approximation to be valid for defects whose geometric features are smooth, i.e., that do not have a content at wavelengths shorter than the exchange length.

### B. Linear spin wave modes

The magnetization to linear order in these media may be written as

$$\vec{M}(\vec{x}, t) \simeq M_s\hat{z} + \vec{m}(\vec{x}, t), \quad (2)$$

with  $\vec{m}(\vec{x}, t) = m_x\hat{x} + m_y\hat{y}$ , i.e., perpendicular to  $\hat{z}$ , the equilibrium magnetization direction. Under these conditions we will determine linear surface eigenmodes of frequency  $\omega$ , as follows:

$$\vec{m}(\vec{x}, t) = \text{Re}[\vec{m}^\omega(x, y)e^{-i\omega t}]. \quad (3)$$

### 1. Landau-Lifshitz equation

We are considering a micromagnetic continuum model of description of the magnetization dynamics, which is governed by the Landau-Lifshitz equation of motion for the magnetization. In the magnetostatic approximation that we are considering the effective field that exerts torque on the magnetization is given by the sum of the applied magnetic field  $H_0\hat{z}$  and by the demagnetizing field  $\vec{h}_D(\vec{m})$  produced by the dynamic magnetization. Then, the linear spin wave modes of Eq. (3) satisfy the following Landau-Lifshitz equation written to linear order:

$$i(\omega/|\gamma|)\vec{m} = (M_s\hat{z} + \vec{m}) \times (H_0\hat{z} + \vec{h}_D). \quad (4)$$

This leads to a linear relation between the components of the demagnetizing field and the dynamic magnetization:

$$\begin{pmatrix} h_D^x \\ h_D^y \end{pmatrix} = \begin{pmatrix} h_0 & i\Omega \\ -i\Omega & h_0 \end{pmatrix} \begin{pmatrix} 4\pi m_x \\ 4\pi m_y \end{pmatrix}, \quad (5)$$

with  $h_0 \equiv H_0/4\pi M_s$ . Inverting the previous relations, one obtains the following relation between the components of the dynamic magnetic induction  $\vec{b} = \vec{h}_D + 4\pi\vec{m}$  and those of the demagnetizing field:

$$\begin{pmatrix} b_x \\ b_y \end{pmatrix} = \begin{pmatrix} \mu & i\nu \\ -i\nu & \mu \end{pmatrix} \begin{pmatrix} h_D^x \\ h_D^y \end{pmatrix}, \quad (6)$$

with  $\mu \equiv (h_0^2 + h_0 - \Omega^2)/(h_0^2 - \Omega^2)$  and  $\nu \equiv -\Omega/(h_0^2 - \Omega^2)$  frequency dependent effective susceptibility coefficients. These satisfy

$$\mu - 1 \pm \nu = 1/(h_0 \pm \Omega). \quad (7)$$

### 2. Magnetostatic Maxwell equations and boundary conditions

The magnetic induction  $\vec{b}$  and demagnetizing field  $\vec{h}_D$  that the linear spin wave modes produce should satisfy the following Maxwell equations in the magnetostatic approximation:

$$\nabla \cdot \vec{b} = 0, \quad \nabla \times \vec{h}_D = 0. \quad (8)$$

The second equation may be solved by introducing a magnetostatic potential  $\phi(\vec{x}, t)$  through  $\vec{h}_D = -\nabla\phi$  and then the first becomes Laplace's equation for the magnetostatic potential both inside and outside the sample [since  $\vec{b} = \vec{h}_D$  outside and by use of Eqs. (6) inside]. The magnetostatic boundary conditions that these fields should satisfy on the surfaces of the ferromagnetic samples are that the normal component of the magnetic induction be continuous, i.e.,  $b_n = \vec{b} \cdot \hat{n}$ , with  $\hat{n}$  the normal to the sample surface, and that the tangential demagnetizing field be continuous or equivalently that the magnetostatic potential be continuous.

## III. ORTHOGONALITY EQUATIONS

Instead of using the standard procedure for solving for the magnetostatic linear spin wave modes, that was explained in the previous section II B, the frequencies of the magnetostatic spin wave modes as well as their amplitudes on the surfaces of the sample may be obtained by solving integral equations satisfied by them that follow from the orthogonal

equations method [32]. These are homogeneous eigenvalue equations that may be thought of as a generalization of Green's-extinction theorem [39] to the equations relevant to this case: this is explained in Appendix A. In the following these integral equations are derived for the magnetostatic normal modes evaluated on the surfaces of the sample.

### A. Integral equations originated from the exterior of the magnetized sample

In the upper outside region of the sample the "auxiliary" functions of the orthogonal equations method may be taken as having the following simple form, characterized by a given wave vector  $k$  and decaying at  $y \rightarrow +\infty$ :

$$\phi_U^{-(\omega,k)} = e^{-ikx} e^{-|k|y}, \quad (9)$$

$$b_U^y = h_U^y = -\partial\phi_U/\partial y = |k|\phi_U, \quad (10)$$

$$b_U^x = h_U^x = -\partial\phi_U/\partial x = ik\phi_U, \quad (11)$$

while those in the lower region as

$$\phi_L^{-(\omega,k)} = e^{-ikx} e^{|k|y}, \quad (12)$$

$$b_L^y = h_L^y = -\partial\phi_L/\partial y = -|k|\phi_L, \quad (13)$$

$$b_L^x = h_L^x = -\partial\phi_L/\partial x = ik\phi_L. \quad (14)$$

Their time dependence is  $\exp(i\omega t)$ . The orthogonality Eq. (A4) in the upper region leads to (surface described by  $y = l + \eta(x)$ ,  $dl = dx\sqrt{1 + \eta'(x)^2}$  the length differential, and  $\hat{n} = [-\eta'(x)\hat{x} + \hat{y}]/\sqrt{1 + \eta'(x)^2}$  the surface normal that points into the vacuum)

$$0 = \int_{-\infty}^{\infty} dx e^{-ikx} e^{-|k|\eta(x)} \{ \sqrt{1 + \eta'(x)^2} b_n[x, l + \eta(x)] + [ik\eta'(x) - |k|]\phi[x, l + \eta(x)] \} \quad (15)$$

and in the lower surface described by  $y = -l + \xi(x)$  ( $\hat{n} = [\xi'(x)\hat{x} - \hat{y}]/\sqrt{1 + \xi'(x)^2}$ ):

$$0 = \int_{-\infty}^{\infty} dx e^{-ikx} e^{|k|\xi(x)} \{ \sqrt{1 + \xi'(x)^2} b_n[x, -l + \xi(x)] - [ik\xi'(x) + |k|]\phi[x, -l + \xi(x)] \}. \quad (16)$$

### B. Orthogonality equations originated from the interior of the magnetized sample

Inside the film the magnetostatic potential  $\phi_i = \phi_{\pm}^{-(\omega,k)}$  of the auxiliary functions satisfies Laplace's equation [it follows from Eqs. (6) and (8)]. We choose a pair of them, associated with a wave vector  $(-k)$ , and with growing and decaying exponential behaviors ( $\pm$  signs) in the  $y$  direction, as follows:

$$\phi_i = \phi_{\pm}^{-(\omega,k)} = e^{-ikx} e^{\pm|k|y}, \quad (17)$$

and it follows that

$$\begin{pmatrix} b_x^\pm \\ b_y^\pm \end{pmatrix} = \begin{pmatrix} \mu & -iv \\ iv & \mu \end{pmatrix} \begin{pmatrix} h_x^\pm \\ h_y^\pm \end{pmatrix} = \begin{pmatrix} i(\mu k \pm \nu|k|) \\ -(vk \pm \mu|k|) \end{pmatrix} \phi_\pm. \quad (18)$$

For the ( $\pm$ ) auxiliary functions the previous orthogonality equations (A7) may be written as

$$\begin{aligned} 0 = & \int_{-\infty}^{\infty} dx e^{-ikx} e^{\pm|k|[l+\eta(x)]} \{\sqrt{1+\eta'(x)^2} b_n[x, l+\eta(x)] \\ & + [(vk \pm \mu|k|) + i\eta'(x)(\mu k \pm \nu|k|)] \phi[x, l+\eta(x)]\} \\ & + \int_{-\infty}^{\infty} dx e^{-ikx} e^{\pm|k|[-l+\xi(x)]} \{\sqrt{1+\xi'(x)^2} b_n[x, -l+\xi(x)] \\ & - [(vk \pm \mu|k|) + i\xi'(x)(\mu k \pm \nu|k|)] \phi[x, -l+\xi(x)]\}. \end{aligned} \quad (19)$$

### C. Set of magnetostatic orthogonality equations in a film with geometric defects

In order to better handle the set of orthogonality equations (15), (16), and (19) for the modes, we define  $B_n^u(x) \equiv \sqrt{1+\eta'(x)^2} b_n[x, l+\eta(x)]$  and  $\Phi^u(x) \equiv \phi[x, l+\eta(x)]$  in the upper surface and similarly  $B_n^d(x) \equiv \sqrt{1+\xi'(x)^2} b_n[x, -l+\xi(x)]$  and  $\Phi^d(x) \equiv \phi[x, -l+\xi(x)]$  in the lower one. Thus Eqs. (15), (16), and (19) become the following system of magnetostatic orthogonality equations:

$$\begin{aligned} 0 = & \int_{-\infty}^{\infty} dx e^{-ikx} e^{-|k|\eta(x)} \{B_n^u(x) + [ik\eta'(x) - |k|] \Phi^u(x)\}, \\ 0 = & \int_{-\infty}^{\infty} dx e^{-ikx} e^{|k|\xi(x)} \{B_n^d(x) - [ik\xi'(x) + |k|] \Phi^d(x)\}, \\ 0 = & \int_{-\infty}^{\infty} dx e^{-ikx} e^{\pm|k|[l+\eta(x)]} \{B_n^u(x) \end{aligned}$$

$$\begin{aligned} & + [(vk \pm \mu|k|) + i\eta'(x)(\mu k \pm \nu|k|)] \Phi^u(x)\} \\ & + \int_{-\infty}^{\infty} dx e^{-ikx} e^{\pm|k|[-l+\xi(x)]} \{B_n^d(x) \\ & - [(vk \pm \mu|k|) + i\xi'(x)(\mu k \pm \nu|k|)] \Phi^d(x)\}. \end{aligned} \quad (20)$$

### D. Even geometric obstacles using symmetry properties

If we consider even geometric obstacles, i.e.,  $\eta(-x) = \eta(x)$  and  $\xi(-x) = \xi(x)$ , one may analyze the spin wave modes in terms of functions with different symmetries with respect to the plane  $x = 0$ , i.e., even or odd. For example, the magnetostatic potential evaluated at the upper surface is separated into even (e) and odd (o) parts:

$$\Phi^u(x) = \Phi_e^u(x) + \Phi_o^u(x). \quad (21)$$

It is convenient to describe even,  $E(x)$ , and odd,  $O(x)$ , functions in terms of cosine,  $E_c(q)$ , and sine,  $O_s(q)$ , Fourier transforms, as follows:

$$\begin{aligned} E(x) &= \frac{1}{\pi} \int_0^{\infty} dq \cos(qx) E_c(q), \\ O(x) &= \frac{1}{\pi} \int_0^{\infty} dq \sin(qx) O_s(q), \\ E_c(q) &= 2 \int_0^{\infty} dx \cos(qx) E(x), \\ O_s(q) &= 2 \int_0^{\infty} dx \sin(qx) O(x), \end{aligned} \quad (22)$$

with more details in Appendix B.

Thus the orthogonality equations for the spin wave modes that follow from the orthogonality Eqs. (20) become [details in Appendix C,  $s(k) \equiv \text{sgn}(k)$ ]

$$\begin{aligned} 0 = & B_e^u(k) - is(k)B_o^u(k) - H_e^u(k) + is(k)H_o^u(k) + \frac{2}{N} \sum_q \{C_u^{-|k|}(k, q)B_e^u(q) - is(k)S_u^{-|k|}(k, q)B_o^u(q) - S_u^{-|k|}(k, q)H_e^u(q) \\ & + is(k)C_u^{-|k|}(k, q)H_o^u(q)\}, \end{aligned} \quad (23)$$

$$\begin{aligned} 0 = & B_e^d(k) - is(k)B_o^d(k) - H_e^d(k) + is(k)H_o^d(k) + \frac{2}{N} \sum_q \{C_d^{|k|}(k, q)B_e^d(q) - is(k)S_d^{|k|}(k, q)B_o^d(q) - S_d^{|k|}(k, q)H_e^d(q) \\ & + is(k)C_d^{|k|}(k, q)H_o^d(q)\}, \end{aligned} \quad (24)$$

$$\begin{aligned} 0 = & e^{\pm|k|l} ([s(k)\Omega \pm h][B_e^u(k) - is(k)B_o^u(k)] + [h \pm s(k)\Omega + 1][H_e^u(k) - is(k)H_o^u(k)] + \frac{2}{N} \sum_q \{[s(k)\Omega \pm h][C_u^{\pm|k|}(k, q)B_e^u(q) \\ & - is(k)S_u^{\pm|k|}(k, q)B_o^u(q)] + [h \pm s(k)\Omega + 1][S_u^{\pm|k|}(k, q)H_e^u(q) - is(k)C_u^{\pm|k|}(k, q)H_o^u(q)]\}) + e^{\mp|k|l} ([s(k)\Omega \pm h][B_e^d(k) \\ & - is(k)B_o^d(k)] - [h \pm s(k)\Omega + 1][H_e^d(k) - is(k)H_o^d(k)] + \frac{2}{N} \sum_q \{[s(k)\Omega \pm h][C_d^{\pm|k|}(k, q)B_e^d(q) \\ & - is(k)S_d^{\pm|k|}(k, q)B_o^d(q)] - [h \pm s(k)\Omega + 1][S_d^{\pm|k|}(k, q)H_e^d(q) - is(k)C_d^{\pm|k|}(k, q)H_o^d(q)]\}), \end{aligned} \quad (25)$$

with

$$\begin{aligned}
C_u^{\pm|k|}(k, q) &\equiv \int_{-\infty}^{\infty} dx \cos(qx) \cos(kx) (e^{\pm|k|\eta(x)} - 1), \\
C_d^{\pm|k|}(k, q) &\equiv \int_{-\infty}^{\infty} dx \cos(qx) \cos(kx) (e^{\pm|k|\xi(x)} - 1), \\
S_u^{\pm|k|}(k, q) &\equiv s(k) \int_{-\infty}^{\infty} dx \sin(qx) \sin(kx) (e^{\pm|k|\eta(x)} - 1), \\
S_d^{\pm|k|}(k, q) &\equiv s(k) \int_{-\infty}^{\infty} dx \sin(qx) \sin(kx) (e^{\pm|k|\xi(x)} - 1).
\end{aligned} \tag{26}$$

The previous orthogonality Eqs. (25) were written in terms of sine and cosine Fourier transforms coefficients (they are the unknowns; notice that they are even in their arguments,  $k$  or  $q$ ; also the eigenvalue  $\Omega$  is an unknown). New variables  $H_e(k) \equiv |k|\Phi_e(k)$ ,  $H_o(k) \equiv |k|\Phi_o(k)$  were introduced, and we also used Eq. (7) that allows at the end to transform the orthogonality equations into a standard matrix eigenvalue problem for the frequency  $\Omega$ . Furthermore, the integrals and transforms were written in their discrete versions, a necessary step for numerical calculations (see Appendix B).

#### E. “Mirror reflected” obstacles along the thickness direction of the film

We also consider “mirror reflected” obstacles along the thickness direction  $y$  (with respect to the plane  $y = 0$ ), which correspond to symmetric perturbations, i.e.,  $\eta(x) = -\xi(x)$ . For them  $C_u^{\pm|k|} = C_d^{\mp|k|} \equiv C_{\pm}$  and also  $S_u^{\pm|k|} = S_d^{\mp|k|} \equiv S_{\pm}$ . Also, we define

$$\begin{aligned}
P_{\pm}(k, q) &= \delta_{k,q} + \frac{2}{N} C_{\pm}(k, q), \\
R_{\pm}(k, q) &= \delta_{k,q} + \frac{2}{N} S_{\pm}(k, q), \\
M_{\pm}(k, q) &= e^{\pm|k|l} P_{\pm}(k, q), \\
N_{\pm}(k, q) &= e^{\pm|k|l} R_{\pm}(k, q).
\end{aligned} \tag{27}$$

Thus, for these mirror reflected obstacles and taking the cases  $s = \text{sgn}(k) = \pm 1$ , the previous orthogonality Eqs. (23)–(25) may be written more compactly as

$$0 = P_- B_e^u - R_- H_e^u, \tag{29}$$

$$0 = R_- B_o^u - P_- H_o^u, \tag{30}$$

$$0 = P_- B_e^d - R_- H_e^d, \tag{31}$$

$$0 = R_- B_o^d - P_- H_o^d, \tag{32}$$

$$\begin{aligned}
0 &= (\Omega + h) [M_+ B_e^u + M_- B_e^d - iN_+ B_o^u - iN_- B_o^d] \\
&+ (h + \Omega + 1) [N_+ H_e^u - N_- H_e^d - iM_+ H_o^u + iM_- H_o^d],
\end{aligned} \tag{33}$$

$$\begin{aligned}
0 &= -(\Omega + h) [M_- B_e^u + M_+ B_e^d + iN_- B_o^u + iN_+ B_o^d] \\
&+ (h + \Omega + 1) [N_- H_e^u - N_+ H_e^d + iM_- H_o^u - iM_+ H_o^d],
\end{aligned} \tag{34}$$

$$\begin{aligned}
0 &= -(\Omega - h) [M_+ B_e^u + M_- B_e^d + iN_+ B_o^u + iN_- B_o^d] \\
&+ (h - \Omega + 1) [N_+ H_e^u - N_- H_e^d + iM_+ H_o^u - iM_- H_o^d],
\end{aligned} \tag{35}$$

$$\begin{aligned}
0 &= (\Omega - h) [M_- B_e^u + M_+ B_e^d - iN_- B_o^u - iN_+ B_o^d] \\
&+ (h - \Omega + 1) [N_- H_e^u - N_+ H_e^d - iM_- H_o^u + iM_+ H_o^d].
\end{aligned} \tag{36}$$

We define symmetric and antisymmetric variables with respect to the thickness direction  $y$ :  $B_e^s = B_e^u + B_e^d$ ,  $B_e^a = B_e^u - B_e^d$ , and analogously for the variables  $B_o$ ,  $H_e$ , and  $H_o$ . Indeed, due to our assumed symmetries of the geometric defects, i.e., a geometry with mirror reflection properties with respect to the planes  $x = 0$  and  $y = 0$ , the modes separate into symmetric and antisymmetric with respect to the inversion transformation  $(x, y) \rightarrow -(x, y)$  and are associated with the variables  $B_e^s, B_o^s, H_e^s, H_o^s$  and  $B_e^a, B_o^a, H_e^a, H_o^a$ , respectively. This happens because, given the applied magnetic field and the assumed form of the defects the system is invariant under the inversion transformation  $(x, y) \rightarrow -(x, y)$  or equivalently by a rotation of the system in  $180^\circ$  with respect to the  $z$  axis. This separation of the problem into the just called symmetric and antisymmetric modes is seen explicitly to happen as follows. Summing Eqs. (33), (34) and Eqs. (35), (36), and also from Eqs. (29), (31) and Eqs. (30), (32), one obtains the following equations:

$$\begin{aligned}
0 &= (\Omega + h) [(M_+ - M_-) B_e^a - i(N_+ + N_-) B_o^s] \\
&+ (h + \Omega + 1) [(N_+ + N_-) H_e^a - i(M_+ - M_-) H_o^s],
\end{aligned} \tag{37}$$

$$\begin{aligned}
0 &= -(\Omega - h) [(M_+ - M_-) B_e^a + i(N_+ + N_-) B_o^s] \\
&+ (h - \Omega + 1) [(N_+ + N_-) H_e^a + i(M_+ - M_-) H_o^s],
\end{aligned} \tag{38}$$

$$0 = P_- B_e^a - R_- H_e^a, \tag{39}$$

$$0 = R_- B_o^s - P_- H_o^s. \tag{40}$$

The previous Eqs. (37)–(40) correspond to modes that are antisymmetric with respect to the inversion symmetry operation. Now, summing and subtracting Eqs. (37) and (38) one obtains

$$0 = -\Omega(N_s B_o^s + M_d H_o^s) - ih(N_s H_e^a + M_d B_e^a) - iN_s H_e^a, \tag{41}$$

$$0 = -\Omega(N_s H_e^a + M_d B_e^a) + ih(N_s B_o^s + M_d H_o^s) + iM_d H_o^s, \tag{42}$$

with

$$N_s \equiv N_+ + N_-, \quad M_d \equiv M_+ - M_-. \tag{43}$$

Defining new variables

$$N_s B_o^s + M_d H_o^s = W H_o^s, \quad N_s H_e^a + M_d B_e^a = X H_e^a, \quad (44)$$

with, from Eqs. (39) and (40),

$$W \equiv N_s V + M_d, \quad X \equiv N_s + M_d T, \quad (45)$$

$$V \equiv R_-^{-1} P_-, \quad T \equiv P_-^{-1} R_-,$$

then Eqs. (41) and (42) may be written as

$$0 = \begin{pmatrix} -\Omega I & -ihI - iN_s X^{-1} \\ iM_d W^{-1} + ihI & -\Omega I \end{pmatrix} \begin{pmatrix} W H_o^s \\ X H_e^a \end{pmatrix}. \quad (46)$$

Notice that from Eqs. (28) the matrices  $M_{\pm}, N_{\pm}$  may be written as

$$M_{\pm} = D_{\pm} P_{\pm}, \quad N_{\pm} = D_{\pm} R_{\pm}, \quad (47)$$

with  $D_{\pm}$  the following diagonal matrices:

$$(D_+)_{mn} = e^{|kl|} \delta_{mn}, \quad (D_-)_{mn} = e^{-|kl|} \delta_{mn}, \\ D_+^{-1} = D_-, \quad D_-^{-1} = D_+. \quad (48)$$

Using Eqs. (43), (45), (47), and (48) one obtains

$$W^{-1} = (R_+ V + P_+)^{-1} D_-, \quad X^{-1} = (R_+ + P_+ T)^{-1} D_-. \quad (49)$$

Finally, Eqs. (46) may be combined into the following eigenvalue problem for antisymmetric modes:

$$0 = ([M_d W^{-1} + hI][N_s X^{-1} + hI] - \Omega^2 I)(X H_e^a). \quad (50)$$

Now, about symmetric modes: subtracting Eqs. (33), (34) and Eqs. (35), (36) between themselves and from Eqs. (29)–(32), one obtains the following equations for this type of mode:

$$0 = (\Omega + h)[(M_+ + M_-)B_e^s - i(N_+ - N_-)B_o^a] \\ + (h + \Omega + 1)[(N_+ - N_-)H_e^s - i(M_+ + M_-)H_o^a], \quad (51)$$

$$0 = -(\Omega - h)[(M_+ + M_-)B_e^s + i(N_+ - N_-)B_o^a] \\ + (h - \Omega + 1)[(N_+ - N_-)H_e^s + i(M_+ + M_-)H_o^a], \quad (52)$$

$$0 = P_- B_e^s - R_- H_e^s, \quad (53)$$

$$0 = R_- B_o^a - P_- H_o^a. \quad (54)$$

Summing and subtracting Eqs. (51) and (52) one obtains

$$0 = -\Omega(N_d B_o^a + M_s H_o^a) - ih(M_s B_e^s + N_d H_e^s) - iN_d H_e^s, \quad (55)$$

$$0 = -\Omega(M_s B_e^s + N_d H_e^s) + ih(N_d B_o^a + M_s H_o^a) + iM_s H_o^a, \quad (56)$$

where

$$N_d \equiv N_+ - N_-, \quad M_s \equiv M_+ + M_-. \quad (57)$$

We define new variables

$$N_d B_o^a + M_s H_o^a = Y H_o^a, \quad M_s B_e^s + N_d H_e^s = Z H_e^s, \quad (58)$$

with, from Eqs. (45), (53), (54), and (58),

$$Y \equiv N_d V + M_s, \quad Z \equiv M_s T + N_d. \quad (59)$$

Now, from Eqs. (43), (45), (47), (57), and (59) it results that  $Y = W$  and  $Z = X$ . Equations (55) and (56) may then be written as

$$0 = \begin{pmatrix} -\Omega I & -ihI - iN_d X^{-1} \\ iM_s W^{-1} + ihI & -\Omega I \end{pmatrix} \begin{pmatrix} W H_o^a \\ X H_e^s \end{pmatrix}. \quad (60)$$

These equations may be combined into the following eigenvalue problem for the symmetric modes:

$$0 = ([M_s W^{-1} + hI][N_d X^{-1} + hI] - \Omega^2 I)(X H_e^s). \quad (61)$$

#### IV. SCATTERING, REFLECTION, AND TRANSMISSION COEFFICIENTS

Far from the region of geometric defects, the spin wave mode solutions correspond to those of flat surfaces (see Appendix E). There a plane wave with a specified wave vector  $k$ , and with related amplitudes of the magnetization and magnetostatic fields that vary along the thickness direction  $y$ , is a valid spin wave solution at a frequency  $\omega(k)$  given by the dispersion relation of Eq. (1). Thus a scattering type of solution, with incident, reflected, and transmitted parts that are plane waves of wave vector  $k$ , may be regarded as a spin wave mode solution at frequency  $\omega$ , and far from the geometric defect its magnetostatic potential takes the following form:

$$\phi_{-\infty} = A_I f(y) e^{i(kx - \omega t)} + A_R g(y) e^{-i(kx + \omega t)} : \quad x \rightarrow -\infty, \\ \phi_{\infty} = A_T f(y) e^{i(kx - \omega t)} : \quad x \rightarrow \infty. \quad (62)$$

Notice that the magnetostatic potential profiles of the incident and transmitted waves,  $f(y)$ , are the same, while that of the reflected wave,  $g(y)$ , satisfies  $g(y) = f(-y)$ , i.e., there is a mirror reflection symmetry with respect to the plane  $y = 0$  in the magnetostatic potential between right and left propagating spin wave modes (shape nonreciprocity; see Appendix E).

Now we discuss the reflection and transmission of energy due to scattering, which allows one to evaluate reflection ( $R$ ) and transmission coefficients ( $T$ ). Due to conservation of energy we will verify that  $R + T = 1$ . According to Refs. [3,38] in the magnetostatic approximation the following expression represents the averaged over time energy current density  $\langle \vec{F} \rangle$  of spin waves [it is basically the electromagnetic Poynting vector; a time dependence of the fields as  $\exp(-i\omega t)$  has been assumed]:

$$\langle \vec{F} \rangle = -\frac{c\omega}{8\pi} \text{Re}(i\phi^* \vec{b}), \quad (63)$$

with  $\phi$  and  $\vec{b} = \vec{h}_D + 4\pi \vec{m}$  the magnetostatic potential and magnetic induction associated with the spin wave, respectively. Indeed local conservation of energy is represented by a continuity equation of the form

$$0 = \partial u / \partial t + \nabla \cdot \vec{F}, \quad (64)$$

with  $u$  the energy density. We integrate the previous continuity equation over the volume  $V$  of the film for a stationary process occurring at frequency  $\omega$  and we average over time, the integration over  $\partial u / \partial t$  averaged over time is zero (stationary

process), and we get through Gauss's theorem:

$$0 = \int_V \nabla \cdot (\vec{F}) = \int_S \langle \vec{F} \rangle \cdot d\vec{S}. \quad (65)$$

The integration over the upper and lower surfaces of the film is zero [given the form of  $\langle \vec{F} \rangle$  from Eq. (63) and a similar analysis to what we presented for the extinction theorem in Appendix A 2]. Thus, from the remaining integration over the left and right cross sections of the film, Eq. (65) implies

$$\int dz \int dy \langle F_x \rangle_{-\infty} = \int dz \int dy \langle F_x \rangle_{\infty}, \quad (66)$$

where the integration is over the cross sections at  $x \rightarrow \mp\infty$  of the film (due to translation invariance in the  $z$  direction, the integration in that direction cancels out). Thus, in Eq. (66), the equal sign has come from conservation of energy [Eq. (64)]. The integrals in Eq. (66) may be done using Eqs. (6) and (63). Indeed,

$$\int dy \langle F_x \rangle = -\frac{c\omega}{16\pi} \int dy \left[ 2\mu k |\phi|^2 + \nu \frac{\partial}{\partial y} (|\phi|^2) \right]. \quad (67)$$

Then, according to Eqs. (62) and (67),

$$\int dy \langle F_x \rangle_{\infty} = -|A_T|^2 \frac{c\omega}{16\pi} \{ 2\mu k w [ |f|^2 ] + \nu [ |f(l)|^2 - |f(-l)|^2 ] \}, \quad (68)$$

with

$$w [ |f|^2 ] \equiv \int_{-l}^l dy |f(y)|^2. \quad (69)$$

Furthermore,

$$\begin{aligned} \int dy \langle F_x \rangle_{-\infty} &= -|A_I|^2 \frac{c\omega}{16\pi} \{ 2\mu k w [ |f|^2 ] + \nu [ |f(l)|^2 \\ &\quad - |f(-l)|^2 ] \} - |A_R|^2 \frac{c\omega}{16\pi} \{ -2\mu k w [ |g|^2 ] \\ &\quad + \nu [ |g(l)|^2 - |g(-l)|^2 ] \}. \end{aligned} \quad (70)$$

Using Eqs. (66), (68), and (70), and that  $[ |g|^2 ] = [ |f|^2 ]$  and  $g(\pm l) = f(\mp l)$ , one gets

$$|A_I|^2 - |A_R|^2 = |A_T|^2 \quad (71)$$

or, defining  $|A_R/A_I|^2 = R$  and  $|A_T/A_I|^2 = T$  as reflection and transmission coefficients, one gets

$$R + T = 1 \quad (72)$$

as expected due to energy conservation.

### A. Even and odd modes in 1D and phase shifts

A convenient way to handle numerically the previous scattering problem is to introduce mode solutions at frequency  $\omega$  with parity properties.

First, we present a simple scattering problem for a scalar field in 1D,  $\psi(x)$ , as a useful introduction. The incident, reflected, and transmitted solutions far from the scatterer in

this case are

$$\begin{aligned} \psi_{-\infty} &= A_I e^{i(kx - \omega t)} + A_R e^{-i(kx + \omega t)} : x \rightarrow -\infty, \\ \psi_{\infty} &= A_T e^{i(kx - \omega t)} : x \rightarrow \infty \end{aligned} \quad (73)$$

or equivalently

$$\begin{aligned} \psi_{-\infty} &= e^{-i\omega t} \{ (A_I + A_R) \cos(kx) + (A_I - A_R) i \sin(kx) \}, \\ \psi_{\infty} &= e^{-i\omega t} A_T \{ \cos(kx) + i \sin(kx) \}. \end{aligned} \quad (74)$$

In terms of modes with symmetry properties, the scattering solutions of Eq. (73), that are associated with a wave vector  $k$ , read

$$\begin{aligned} \psi_{-\infty} &= e^{-i\omega t} \{ C_e \cos(kx - \delta_e) + C_o \sin(kx - \delta_o) \}, \\ \psi_{\infty} &= e^{-i\omega t} \{ C_e \cos(kx + \delta_e) + C_o \sin(kx + \delta_o) \}, \end{aligned} \quad (75)$$

where  $\delta_e$  and  $\delta_o$  are phase shifts produced by the scatterer in the even and odd solutions. From Eqs. (74) and (75) by simple algebra one gets

$$\begin{aligned} A_I &= -iC_o e^{-i\delta_o}, \quad A_R = C_o e^{i\delta_e} \sin(\delta_e - \delta_o), \\ A_T &= -iC_o e^{i\delta_e} \cos(\delta_e - \delta_o), \quad C_e = -iC_o e^{i(\delta_e - \delta_o)}, \end{aligned} \quad (76)$$

from which it follows that

$$|A_R/A_I|^2 = \sin^2(\delta_e - \delta_o), \quad |A_T/A_I|^2 = \cos^2(\delta_e - \delta_o). \quad (77)$$

Thus the reflection and transmission coefficients may be determined through the difference of phase shifts associated with even and odd modes.

### B. Film modes with symmetry properties and phase shifts

The scattering modes' solutions for the magnetostatic potential  $\phi_{-\infty}(x, y, t)$  of Eqs. (62) at  $x \rightarrow -\infty$  may be written as

$$\begin{aligned} \phi_{-\infty} &= e^{-i\omega t} \{ A_I f(y) e^{ikx} + A_R f(-y) e^{-ikx} \} \\ &= e^{-i\omega t} \{ e(y) [ (A_I + A_R) \cos(kx) + (A_I - A_R) i \sin(kx) ] \\ &\quad + o(y) [ (A_I - A_R) \cos(kx) + (A_I + A_R) i \sin(kx) ] \}, \end{aligned} \quad (78)$$

with

$$e(y) \equiv [f(y) + f(-y)]/2, \quad o(y) \equiv [f(y) - f(-y)]/2 \quad (79)$$

even and odd functions along the thickness of the film, respectively. Similarly,

$$\begin{aligned} \phi_{\infty} &= e^{-i\omega t} A_T f(y) e^{ikx} \\ &= e^{-i\omega t} A_T [e(y) + o(y)] [\cos(kx) + i \sin(kx)]. \end{aligned} \quad (80)$$

A convenient way to handle numerically the previous scattering problem is to introduce mode solutions at frequency  $\omega$  with symmetry properties, similarly as in Eqs. (75):

$$\begin{aligned} \phi_{-\infty} &= e^{-i\omega t} \{ e(y) [ C_e^e \cos(kx - \delta_e^e) + C_o^e \sin(kx - \delta_o^e) ] \\ &\quad + o(y) [ C_e^o \cos(kx - \delta_e^o) + C_o^o \sin(kx - \delta_o^o) ] \}, \end{aligned} \quad (81)$$

$$\begin{aligned} \phi_{\infty} &= e^{-i\omega t} \{ e(y) [ C_e^e \cos(kx + \delta_e^e) + C_o^e \sin(kx + \delta_o^e) ] \\ &\quad + o(y) [ C_e^o \cos(kx + \delta_e^o) + C_o^o \sin(kx + \delta_o^o) ] \}, \end{aligned} \quad (82)$$

i.e., we are distinguishing even-even ( $C_e^e$ ), even-odd ( $C_e^o$ ), odd-even ( $C_o^e$ ), and odd-odd ( $C_o^o$ ) modes, considering parity properties in the  $y$  and  $x$  directions, respectively. Similarly to what was done in the previous section, comparing Eqs. (78), (81) and Eqs. (80), (82) for the different types of modes, one obtains

$$\begin{aligned} A_I &= -iC_o^e e^{-i\delta_o^e}, & A_R &= C_o^e e^{i\delta_e^e} \sin(\delta_e^e - \delta_o^e), \\ A_T &= -iC_o^e e^{i\delta_e^e} \cos(\delta_e^e - \delta_o^e), & C_e^e &= -iC_o^e e^{i(\delta_e^e - \delta_o^e)} \end{aligned} \quad (83)$$

and

$$\begin{aligned} A_I &= -iC_o^o e^{-i\delta_o^o}, & A_R &= -C_o^o e^{i\delta_e^o} \sin(\delta_e^o - \delta_o^o), \\ A_T &= -iC_o^o e^{i\delta_e^o} \cos(\delta_e^o - \delta_o^o), & C_e^o &= -iC_o^o e^{i(\delta_e^o - \delta_o^o)}. \end{aligned} \quad (84)$$

Notice that Eqs. (83), (84) are consistent if  $C_o^o = C_o^e e^{i(\delta_e^e - \delta_o^e)}$ ,  $\delta_e^o = \delta_o^e$ , and  $\delta_o^o = \delta_e^e$ . Indeed calling  $\delta_e^e = \delta_s$ ,  $\delta_o^e = \delta_a$ , and  $C_o^e = C_a$ , then

$$\begin{aligned} A_I &= -iC_a e^{-i\delta_a}, \\ A_R &= C_a e^{i\delta_s} \sin(\delta_s - \delta_a), \\ A_T &= -iC_a e^{i\delta_s} \cos(\delta_s - \delta_a). \end{aligned} \quad (85)$$

Also, notice that  $C_a e^{i\delta_s} = iC_s e^{i\delta_a}$ , with  $C_s \equiv C_e^e$ . Then Eqs. (81) and (82) take the form

$$\begin{aligned} \phi_{-\infty} &= A_I e^{-i\omega t} \{e(y)[e^{i\delta_s} \cos(kx - \delta_s) + i e^{i\delta_a} \sin(kx - \delta_a)] \\ &\quad + o(y)[e^{i\delta_a} \cos(kx - \delta_a) + i e^{i\delta_s} \sin(kx - \delta_s)]\}, \end{aligned} \quad (86)$$

$$\begin{aligned} \phi_{\infty} &= A_I e^{-i\omega t} \{e(y)[e^{i\delta_s} \cos(kx + \delta_s) + i e^{i\delta_a} \sin(kx + \delta_a)] \\ &\quad + o(y)[e^{i\delta_a} \cos(kx + \delta_a) + i e^{i\delta_s} \sin(kx + \delta_s)]\}. \end{aligned} \quad (87)$$

Then, the previous solutions at  $x = \pm\infty$  may be written as

$$\begin{aligned} \phi_{-\infty} &= A_I e^{-i\omega t} \{e^{i\delta_s} [e(y) \cos(kx - \delta_s) + i o(y) \sin(kx - \delta_s)] \\ &\quad + e^{i\delta_a} [o(y) \cos(kx - \delta_a) + i e(y) \sin(kx - \delta_a)]\}, \end{aligned} \quad (88)$$

$$\begin{aligned} \phi_{\infty} &= A_I e^{-i\omega t} \{e^{i\delta_s} [e(y) \cos(kx + \delta_s) + i o(y) \sin(kx + \delta_s)] \\ &\quad + e^{i\delta_a} [o(y) \cos(kx + \delta_a) + i e(y) \sin(kx + \delta_a)]\}. \end{aligned} \quad (89)$$

Thus the solutions involve sums of symmetric and antisymmetric solutions under the inversion symmetry of the system, i.e.,  $(x, y) \rightarrow -(x, y)$ , that we call  $\phi_s$  and  $\phi_a$ , respectively. Indeed in our case the solution for the potential in all the regions may then be written as

$$\phi(x, y) = A_I e^{-i\omega t} \{e^{i\delta_s} \phi_s(x, y) + e^{i\delta_a} \phi_a(x, y)\}, \quad (90)$$

with the following behavior of the symmetric and antisymmetric solutions for the magnetostatic potential at  $x \rightarrow \pm\infty$ :

$$\begin{aligned} \phi_s^{\pm\infty}(x, y) &= e(y) \cos(kx \pm \delta_s) + i o(y) \sin(kx \pm \delta_s), \\ \phi_a^{\pm\infty}(x, y) &= o(y) \cos(kx \pm \delta_a) + i e(y) \sin(kx \pm \delta_a). \end{aligned} \quad (91)$$

These symmetric and antisymmetric solutions have clear phase shifts  $\delta_s$  and  $\delta_a$  at  $|x| \rightarrow \infty$ , respectively. Furthermore, from Eqs. (85) one concludes that

$$\begin{aligned} R &= |A_R/A_I|^2 = \sin^2(\delta_s - \delta_a), \\ T &= |A_T/A_I|^2 = \cos^2(\delta_s - \delta_a). \end{aligned} \quad (92)$$

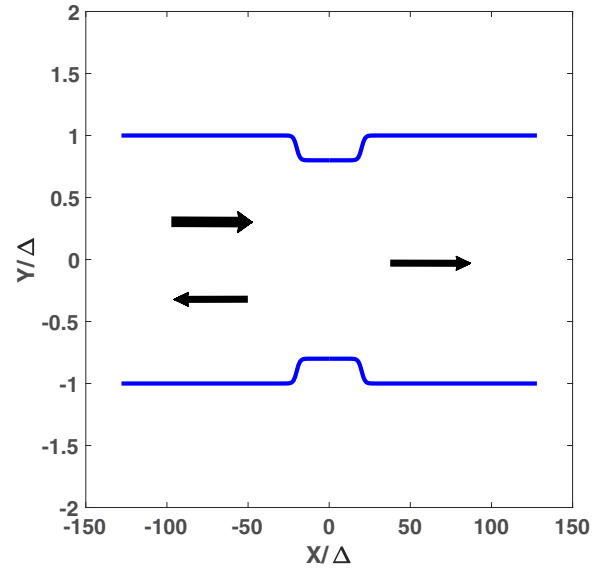


FIG. 1. Geometric defects chosen: schematics of depressions symmetrically located in the film. Approximate dimensions of the depressions in this figure: depth  $p = 0.1\Delta$ , length  $2a = 40\Delta$ , and transition regions scale  $b = 2\Delta$ .

Thus the reflection ( $R$ ) and transmission ( $T$ ) coefficients may be calculated using the differences of the phase shifts of the just mentioned symmetric and antisymmetric modes—phase shifts that are produced by the geometric defects.

Notice that for a film with flat surfaces these symmetric ( $S$ ) and antisymmetric ( $A$ ) mode solutions for the magnetostatic potential are

$$\begin{aligned} \phi_s^f(x, y) &= S(x, y) = e(y) \cos(kx) + i o(y) \sin(kx), \\ \phi_a^f(x, y) &= A(x, y) = o(y) \cos(kx) + i e(y) \sin(kx). \end{aligned} \quad (93)$$

These are simply interpreted, since they are basically the sum and difference of right and left traveling spin wave modes (here we write just the magnetostatic potential of the spin wave):

$$\begin{aligned} S(x, y) &= [f(y)e^{ikx} + f(-y)e^{-ikx}]/2, \\ A(x, y) &= [f(y)e^{ikx} - f(-y)e^{-ikx}]/2. \end{aligned} \quad (94)$$

## V. EXAMPLES OF MAGNETOSTATIC SURFACE SCATTERING

In Sec. II A the geometric defects were presented as modifying the upper and lower surfaces of the film as  $y = l + \eta(x)$  and  $y = -l + \xi(x)$ , respectively. In order to present examples of magnetostatic surface scattering using the theory presented, we chose a symmetric configuration with  $\eta(x) = -\xi(x) = p\{-1 + \tanh[(x - a)/b]\}$  (formulas valid for  $x \geq 0$  and with reflection symmetry with respect to  $x = 0$ ). Figure 1 represents the film with these depressions for the case  $a = 20\Delta$ , with  $\Delta$  the smallest length with which we discretize numerical results (we also present calculations with  $a = 10\Delta$ ), and we took  $b = 2\Delta$  and  $p = 0.1\Delta$  for this figure: these correspond to symmetrically located depressions (we also calculated an example with  $b = 5\Delta$ ).

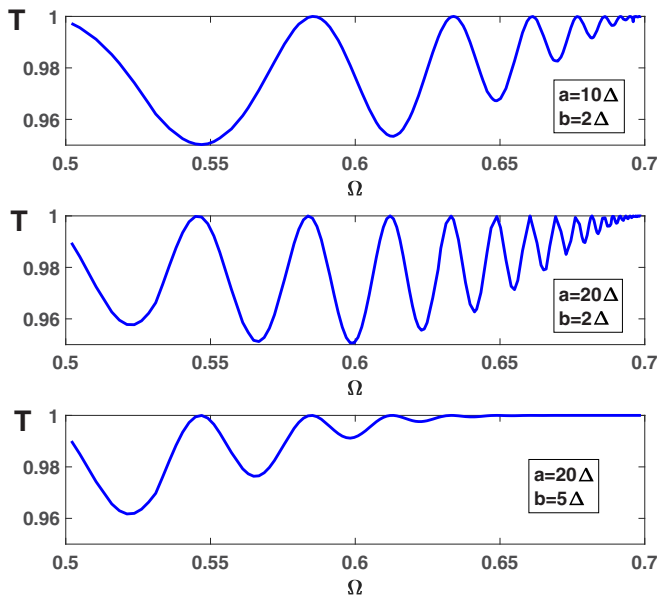


FIG. 2. Scattering transmission coefficient  $T$  as a function of surface mode frequency,  $\Omega = \omega/4\pi M_s |\gamma|$ , for different cases of depression half widths ( $a$ ) and transition distances ( $b$ ):  $a = 10\Delta$ ,  $b = 2\Delta$ ,  $a = 20\Delta$ ,  $b = 2\Delta$ , and  $a = 20\Delta$ ,  $b = 5\Delta$ , respectively ( $h_0 = H_0/4\pi M_s = 0.2$  and  $p = 0.1\Delta$ ).

The calculations that will be presented in the following are done for films of length between  $-L \leq x \leq L$ , with  $L = 1024\Delta$ , so Fig. 1 is just a section of the full length, shown for illustrative purposes.  $\Delta$  is a unit of length, so wave vectors will have units of  $1/\Delta$ . The thickness of the film is taken between  $y = -\Delta$  and  $y = \Delta$ . All the results that we present have no units; for example, for the coordinate  $x$  actually we plot  $x/\Delta$ : indeed magnetostatic equations are independent of  $\Delta$ ; there is no underlying length scale (the only length scale is the thickness of the film). Also, we take  $h_0 = H_0/4\pi M_s = 0.2$ , so that the range of frequencies of the Damon-Eshbach modes in this case is between the normalized frequencies  $\Omega_l = \sqrt{h_0(h_0 + 1)} \simeq 0.49$  and  $\Omega_u = h_0 + 1/2 = 0.7$ .

First, we discuss results on scattering of propagating magnetostatic surface modes. As presented in the theory sections, our theory is able to calculate the scattering of an incident magnetostatic surface wave of wave vector  $k$ , with an associated wavelength  $\lambda = 2\pi/k$ . Reflection ( $R$ ) and transmission coefficients ( $T$ ) of this incident surface wave were determined through the phase shifts  $\delta_s$  and  $\delta_a$  of modes symmetric and antisymmetric under inversion, as shown in Eqs. (92). Then, the transmission coefficient is given by  $T = \cos^2 \delta$ , where we have defined  $\delta \equiv \delta_s - \delta_a$ .

In Fig. 2 the transmission coefficient  $T$  is shown as a function of normalized frequency [frequency  $\Omega \equiv \omega/4\pi M_s |\gamma|$  and wave vector  $k$  are related through Eq. (1) for these scattering modes] for three examples of depressions. According to Fig. 2 these particular obstacles do not affect much the overall transmission ( $T$  hovers between 0.95 and 1), but interestingly there are particular frequencies at which there is perfect transmission ( $T = 1$ ), which we associate with resonances [35,40]. Resonances have been qualitatively associated with a wave being trapped for a while through successive reflections in

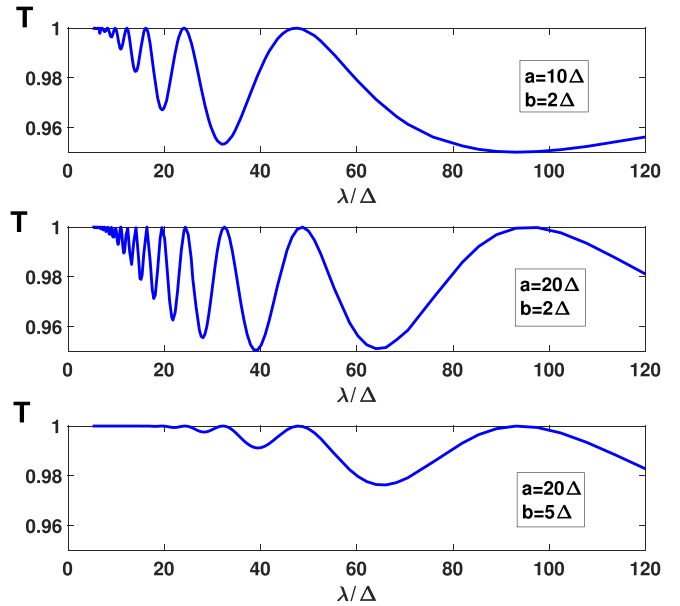


FIG. 3. Scattering transmission coefficient  $T$  as a function of surface mode wavelength  $\lambda$  (scaled by  $\Delta$ ) for different cases of depression half widths ( $a$ ) and transition distances ( $b$ ):  $a = 10\Delta$ ,  $b = 2\Delta$ ,  $a = 20\Delta$ ,  $b = 2\Delta$ , and  $a = 20\Delta$ ,  $b = 5\Delta$ , respectively ( $h_0 = H_0/4\pi M_s = 0.2$  and  $p = 0.1\Delta$ ).

a “potential well” and then escaping from it; the frequency width of these resonances would be proportional to the inverse “trapping time” (a bound state would be very difficult to spot as a transmission resonance, since it should have an infinitesimal frequency width). Notice that the lowest subplots of Fig. 2, which correspond to the same approximate size of depression ( $a = 20\Delta$ ) but to different transition sizes ( $b = 2\Delta$ , or a “sharp” depression, and  $b = 5\Delta$ , or an “extended” depression), do share the same frequency resonances while the extended depression results may be interpreted in terms of shorter trapping times or wider resonance widths: this was to be expected of a “looser” depression—an interpretation also consistent with the “disappearance” of resonances at higher frequencies in the latter case. Also notice that between the first two subplots the size of the depression ( $a$ ) is doubled, keeping the transition regions equal ( $b$ ): new resonances appear for the larger size of depression as to be expected, but also some of them are repeated with the other case (due to sizes of depressions that differ by a factor of two approximately).

In Fig. 3, where the transmission coefficient is plotted versus wavelength for the same previous cases, an interpretation of the results becomes more clear. The first two subplots, where  $a$  changes from  $a = 10\Delta$  to  $a = 20\Delta$ , keeping  $b = 2\Delta$  the same, show resonances at approximately  $\lambda/\Delta = 47.5, 24, 16, 12.3$  and at  $\lambda/\Delta = 95.5, 49, 32.5, 24.5, 19.5, 16.5, 14, 12.3, \dots$ , respectively, i.e., there are some coincidences. For the first subplot, i.e.,  $a = 10\Delta$ , the longest wavelength resonance at  $\lambda/\Delta = 47.5$  may be interpreted as half the wavelength coinciding with an approximate size of the depression [ $2(a + b) = 24\Delta$ ], the second resonance  $\lambda/\Delta = 24$  corresponds to the full wavelength fitting with the size of the depression, the third resonance at  $\lambda/\Delta = 16$  when  $3/2$  of the wavelength

coincides approximately with the depression size, and the fourth resonance at  $\lambda/\Delta = 12.3$  when twice the wavelength coincides with the depression size, .... For the case of the second subplot ( $a = 20\Delta$ ,  $b = 2\Delta$ ) of approximate depression size  $44\Delta$  (or apparently better  $48\Delta$ ) a similar explanation of the longest wavelength resonances at  $\lambda/\Delta = 95.5, 49, 32.5, 24.5$  may be given: they occur approximately when  $1/2, 1, 3/2, 2$  of the respective wavelengths coincide with the approximate size of the depression. Thus the depressions would effectively act similarly to potential wells, since resonances occur when appropriate fractions of the wavelength “fit” with the depressions’ sizes.

The previous transmission coefficients were calculated by determining the phase shifts  $\delta_s$ ,  $\delta_a$ , associated with the symmetric and antisymmetric modes under inversion. In the following we comment about the determination of these phase shifts with our method. The phase shifts  $\delta_a$ ,  $\delta_s$  are determined by plotting the inverse cosine transforms associated with the even functions  $H_e^a$  and  $H_e^s$  of Eqs. (50) and (61), respectively. In both cases (symmetric and antisymmetric modes) we plot the inverse Fourier cosine transforms for no geometric defects and with them, and then we determine the phase shifts between these plots at a distance  $x \sim 100\Delta$  from the center  $x = 0$ , i.e., approximately at the right end of Fig. 1. Notice that the parameter  $L$ , that reflects the end of an actual film and that needs to be taken as finite in a numerical calculation, is a “regulator” for the problem, i.e., it discretizes the number of modes and allows one to count them. Also, due to this regulator the inverse Fourier cosine transforms have zero derivatives at  $x = L$  and the plots of  $H_e^a(x)$  and  $H_e^s(x)$  coincide at  $x = L$  for the film with and without defects, meaning that the phase shifts determined at  $x = L$  are zero; that is why in our case we determine these phase shifts closer to the defects, i.e., at approximately  $x = L/10$ .

Figure 4 plots the difference of phase shifts of symmetric and antisymmetric modes, i.e.,  $\delta \equiv \delta_s - \delta_a$ , as a function of the wavelength of the incident magnetostatic surface wave. Clearly  $\delta$  oscillates in a nonuniform way as a function of  $\lambda$ . Peaks of these oscillations represent lower transmissions and zeros represent full transmission or resonances. These oscillations of  $\delta$  between positive and negative values of the curves of Fig. 4 imply directly the recurrence of full transmissions of Figs. 2 and 3.

Now we turn to discussing the appearance of localized modes associated with the presence of these geometric defects which are depressions. Indeed for both extensions of the depressions, i.e.,  $a = 10\Delta, 20\Delta$ , extensions of the transition regions  $b = 2\Delta, 5\Delta$ , and for the given depth  $p = 0.1\Delta$ , interestingly there are two localized modes appearing close to the region of the depressions. In all these cases there is a mode of lower frequency that is localized mainly in the interior of the depressions and a higher frequency mode localized in the interior and in the contiguous region to the depression. Figure 5 is a plot of the shapes of  $H_e^a$  for the lowest frequency localized antisymmetric modes, with  $a = 10\Delta, b = 2\Delta$ ,  $a = 20\Delta, b = 2\Delta$ , and  $a = 20\Delta, b = 5\Delta$ , respectively. Clearly these previous modes are approximately localized to the regions limited by  $x = 10\Delta, 20\Delta$ , when  $a = 10\Delta, 20\Delta$ , respectively. A comparison of the last two subplots, at the same value of  $a = 20\Delta$  and varying  $b = 2\Delta, 5\Delta$ , respectively, shows that

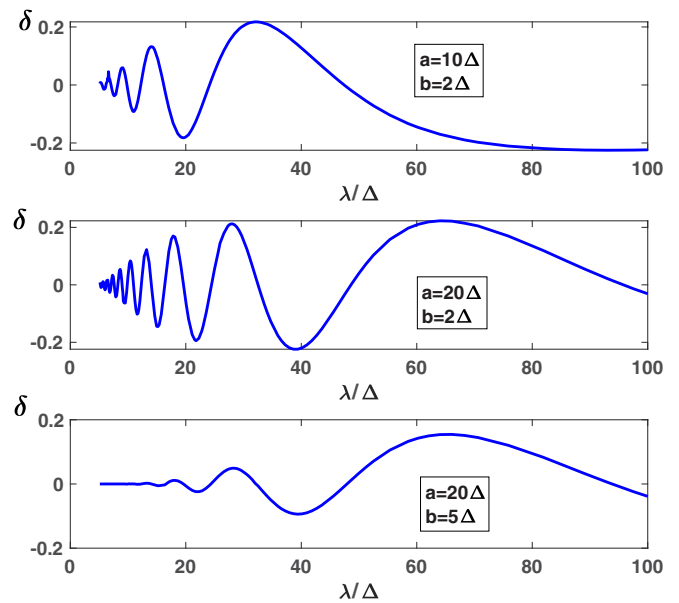


FIG. 4. Scattering phase shift  $\delta \equiv \delta_s - \delta_a$  as a function of surface mode wavelength  $\lambda = 2\pi/k$  (scaled by  $\Delta$ ), for different cases of depression half widths ( $a$ ) and transition distances ( $b$ ):  $a = 10\Delta, b = 2\Delta$ ,  $a = 20\Delta, b = 2\Delta$ , and  $a = 20\Delta, b = 5\Delta$ , respectively.

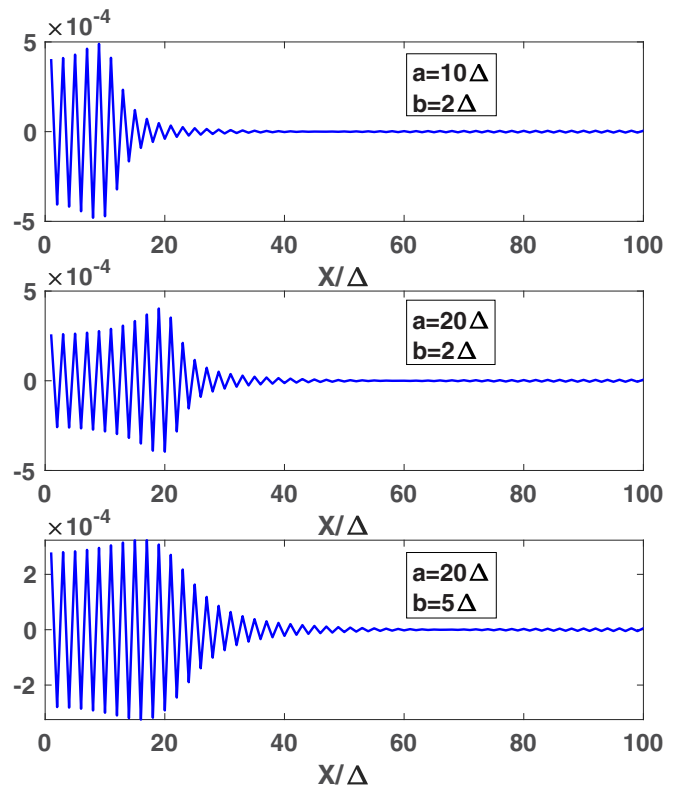


FIG. 5. Shapes of the lowest frequency localized antisymmetric modes (variable  $H_e^a$ ) as a function of the distance from the center  $x = 0$  of the film, for different cases of depression half widths ( $a$ ) and transition distances ( $b$ ):  $a = 10\Delta, b = 2\Delta$ ,  $a = 20\Delta, b = 2\Delta$ , and  $a = 20\Delta, b = 5\Delta$ , respectively.

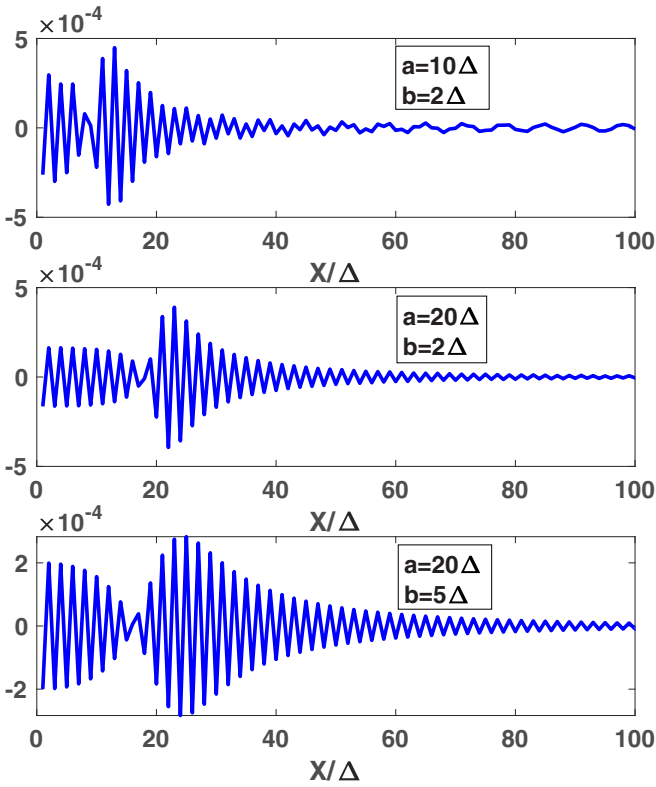


FIG. 6. Shapes of the second lowest frequency localized symmetric modes (variable  $H_e^s$ ) as a function of the distance from the center  $x = 0$  of the film, for different cases of depression half widths ( $a$ ) and transition distances ( $b$ ):  $a = 10\Delta$ ,  $b = 2\Delta$ ,  $a = 20\Delta$ ,  $b = 2\Delta$ , and  $a = 20\Delta$ ,  $b = 5\Delta$ , respectively.

with a looser depression ( $b = 5\Delta$ ) the localized mode extends a little further out, as one would have expected.

Figure 6 is a plot of the shapes of  $H_e^s$  for the second lowest frequency localized symmetric modes, for the same previous choice of geometric parameters. These “second” localized symmetric modes do have amplitudes in the interior regions of the depressions and decaying amplitudes outside the depressions of an extent similar to the interior regions.

The localized modes at the depressions do have cosine Fourier transform coefficients of higher amplitudes at the higher end of the wave-vector range, as evidenced in Fig. 7. Thus these modes do have a short wavelength content in their structure, which allows them to be localized at the depressions (they also oscillate quite a bit inside them).

Similar scattering calculations were done for a semi-infinite medium (theory explained in Appendix D) and we did find that there are very similar localized modes at their surface when there is a single analogous depression. One would expect a finite thickness effect of the film if the depressions had a higher depth. All this is consistent with the short wavelength content of these localized modes.

Furthermore in Fig. 8 the frequencies of the two symmetric localized modes are plotted in terms of a variable depth  $p$  of the depressions. Thus there is a monotonic decrease of the frequencies of these localized modes as the depth of the depressions increases. The decrease starts at the frequency of the surface modes of a perfect semi-infinite surface (or short

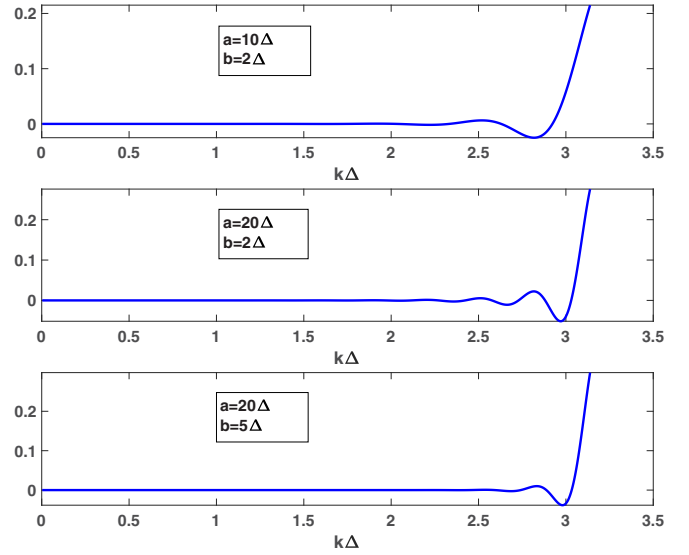


FIG. 7. Cosine Fourier transform coefficients of the lowest frequency localized symmetric modes (variable  $H_e^s$ ) as a function of the nondimensional wave vector  $k\Delta$ , for different cases of depression half widths ( $a$ ) and transition distances ( $b$ ):  $a = 10\Delta$ ,  $b = 2\Delta$ ,  $a = 20\Delta$ ,  $b = 2\Delta$ , and  $a = 20\Delta$ ,  $b = 5\Delta$ , respectively.

wavelength limit of a perfect film also), i.e.,  $\Omega_u = h_0 + 1/2 = 0.7$ . The antisymmetric localized modes have similar frequencies of those of the symmetric modes shown in Fig. 8. Notice that these discrete frequencies of localized modes are immersed in the continuum spectrum of the DE surface modes, as in other studies [41].

We make a final comment about the calculations. The eigenvalue problems that are solved, i.e., Eqs. (50) and (61), are diagonal when the film has no defects: then we start the calculations with  $p = 0$  or flat surfaces, the eigenvalues and eigenvectors are very simple, and each one corresponds to a given value of wave vector  $k$ . Then the parameter  $p$  is changed step by step (this allowed us to plot for example the frequencies of Fig. 8) and the different eigenvalues and eigenvectors are followed as they evolve with  $p$  growing: this allows one to identify the effect of the defects in the scattering of a mode with associated wave vector  $k$  at infinity.

Finally, we do give an estimate of the effect of Gilbert damping in this magnetostatic scattering process, specifically for resonances ( $\alpha$  is taken as the Gilbert damping constant). There is a damping decay time,  $\tau = 1/\omega\alpha$  for a spin wave of frequency  $\omega$ , and also an estimate of resonance trapping time is  $T = 1/\Delta\omega$ , with  $\Delta\omega$  the frequency width of the resonance. Then resonance trapping time over damping decay time is given approximately as

$$\frac{T}{\tau} \sim \frac{\Omega\alpha}{\Delta\Omega} \sim \frac{0.5 \times 0.001}{0.02} \sim 0.3, \quad (95)$$

where  $\Omega$  was estimated to be of the order of 0.5; from Fig. 2 we estimated  $\Delta\Omega$  of order 0.02 for a resonance and we took a low damping constant,  $\alpha \sim 0.001$ . Thus this estimate tells us that in low damping ferromagnets it may be possible to see magnetostatic resonances not being significantly affected by damping.

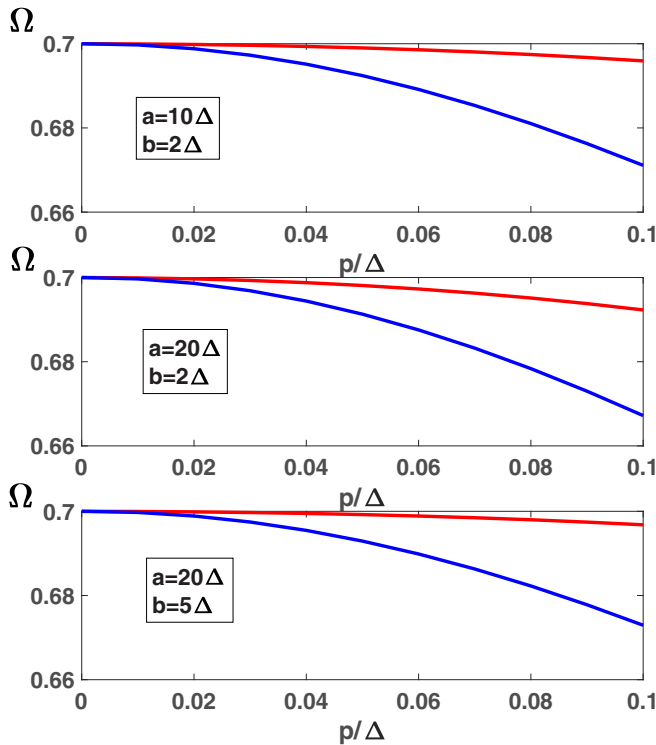


FIG. 8. Normalized frequencies,  $\Omega = \omega/4\pi M_s |\gamma|$ , of the localized symmetric modes as a function of the depth  $p$  of the geometric depressions (the thickness of the film is  $w = 2\Delta$ ), for different cases of depression half widths ( $a$ ) and transition distances ( $b$ ):  $a = 10\Delta$ ,  $b = 2\Delta$ ,  $a = 20\Delta$ ,  $b = 2\Delta$ , and  $a = 20\Delta$ ,  $b = 5\Delta$ , respectively.

## VI. CONCLUSIONS

A study of scattering of magnetostatic Damon-Eshbach (DE) waves by geometric defects was presented. A theory was developed that may be applied to defects of arbitrary shapes in ferromagnetic films and semi-infinite media. This theory is based on an extension of the Green's-extinction theorem: integral equations are obtained for the modes on the surfaces and their frequencies. We chose symmetrically located defects: this allowed us to simplify the scattering calculations, which may be framed in terms of scattering phase shifts of symmetric and antisymmetric modes under inversion (the phase shifts measure how much the solutions are displaced in the flat regions due to the presence of defects in comparison with the case without defects). We calculated transmission coefficients that are directly written in terms of the mentioned phase shifts (it is proven that the sum of the transmission and reflection coefficients is one due to energy conservation in the scattering process). We provided examples of the application of the theory by choosing as geometrical defects symmetrically located depressions: we varied a bit their extent, transition regions, and depth. The results are that the transmission coefficients decrease with depth of the depressions and they show "resonances," i.e., there are particular incident wavelengths (or frequencies) at which there is perfect transmission; this is associated with a wave that is temporarily trapped in the depressions and then leaves. The depressions would effectively act similarly to potential wells, since resonances occur when appropriate fractions of an incoming wavelength

fit with the approximate depression's sizes. Interestingly we also found the appearance of two localized modes for both types of modes (symmetric and antisymmetric under inversion) in the depressions, with frequencies that are lower than the short wavelength limit of DE surface waves in films, i.e., they are bound states in the continuum. The lowest frequency modes are localized inside the depressions, while the higher frequency modes do have localization inside the depression and to a similar extent also they do show amplitude outside the depressions. Very similar localized modes do appear in a semi-infinite medium with depressions, since these modes have a high content of short wavelengths in themselves. The latter indicates that these types of scattering effects should appear in all surfaces with roughness or more pronounced geometric defects.

## ACKNOWLEDGMENTS

We acknowledge support by Fondecyt Project No. 1200829 ANID, (Chile) and ANID/PIA Basal Program for Centers of Excellence, Grant No. AFB 220001 CEDENNA (Chile).

## APPENDIX A: GREEN'S-EXTINCTION THEOREM AND ORTHOGONAL EQUATIONS METHOD

A type of Green's-extinction theorem [39] has been used to obtain spin wave modes in several geometries by the author and co-workers, applied either in the magnetostatic approximation [27–29] or in the dipole-exchange approximation [30–32]. Our initial applications of the method used Green's functions, while the latter studies used auxiliary functions, i.e., an introduced variation of the method, which was named the orthogonal equations method [32] and that is also used in the present work. In the following the main ideas of these methods are summarized.

The initial applications considered interior and exterior sets of Green's functions that satisfy the Landau-Lifshitz magnetization dynamics equations and the magnetostatic Maxwell's equations (i.e., the equations introduced in subsections II B 1 and II B 2, but evaluated at negative frequencies and wave vectors, and without regard to boundary conditions), with the exception that the magnetic inductions satisfy

$$\nabla \cdot \vec{b}_G(\vec{x} - \vec{x}') = 4\pi\delta(\vec{x} - \vec{x}'), \quad (\text{A1})$$

i.e., they consider localized artificial magnetic charges at  $\vec{x}'$ .

### 1. Integral equations outside the magnetized sample

Integral equations can be derived for the linear normal modes of the system if one integrates in the region outside the magnetized sample the following expression:

$$\int_{V_{out}} dV \{ \phi_0^{-\omega}(\vec{x} - \vec{x}') \nabla \cdot \vec{b}^{\omega}(\vec{x}) - \phi^{\omega}(\vec{x}) \nabla \cdot \vec{b}_0^{-\omega}(\vec{x} - \vec{x}') \}, \quad (\text{A2})$$

which involves the modes and the outside Green's function. The volume of integration is chosen outside the magnetized sample, but ending on its limiting surface. Using the equations for the divergences of the magnetic inductions, and since outside  $\vec{b}^{\omega} = -\nabla\phi^{\omega}$  and  $\vec{b}_0^{-\omega} = -\nabla\phi_0^{-\omega}$ , integrating by parts the previous equation one obtains (Green's

theorem)

$$\begin{aligned} \int_S d\vec{S} \cdot \{ \phi_0^{-\omega}(\vec{x} - \vec{x}') \vec{b}^\omega(\vec{x}) - \phi^\omega(\vec{x}) \vec{b}_0^{-\omega}(\vec{x} - \vec{x}') \} \\ = \begin{Bmatrix} 4\pi \phi^\omega(\vec{x}') \\ 0 \end{Bmatrix}, \end{aligned} \quad (\text{A3})$$

with  $S$  the surface of this nonmagnetized region, with its normal pointing out of the sample, and the upper inhomogeneous form applies if  $\vec{x}'$  is chosen outside the magnetized sample and the lower if  $\vec{x}'$  is inside. The latter homogeneous equation is associated with the extinction name, since the integral expression is extinguished in that case.

Analogous homogeneous integral equations may be written if instead of exterior Green's functions one uses auxiliary functions in the outside region that satisfy the same equations as the modes without regard to boundary conditions (evaluated at negative frequencies and wave vectors, no sources). Thus, for these outside auxiliary functions, one gets

$$\int_S d\vec{S} \cdot \{ \phi_o^{-\omega}(\vec{x}) \vec{b}^\omega(\vec{x}) - \phi^\omega(\vec{x}) \vec{b}_o^{-\omega}(\vec{x}) \} = 0. \quad (\text{A4})$$

## 2. Integral equations inside the magnetized sample

In a similar way the following integral is taken over the interior of the magnetized sample volume:

$$0 = \int_{V_{in}} dV \{ \phi_I^{-\omega}(\vec{x}, \vec{x}') \nabla \cdot \vec{b}^\omega - \phi^\omega(\vec{x}) \nabla \cdot \vec{b}_I^{-\omega}(\vec{x}, \vec{x}') \}, \quad (\text{A5})$$

with  $\phi, \vec{b}$  corresponding to normal modes and  $\phi_I, \vec{b}_I$  representing an inside Green's function. Integrating by parts and using the equations for the divergences of the magnetic inductions involved, one obtains

$$\int_S d\vec{S} \cdot \{ \phi^\omega(\vec{x}) \vec{b}_I^{-\omega}(\vec{x}, \vec{x}') - \phi_I^{-\omega}(\vec{x}, \vec{x}') \vec{b}^\omega(\vec{x}) \} = \begin{Bmatrix} 0 \\ 4\pi \phi^\omega(\vec{x}') \end{Bmatrix}. \quad (\text{A6})$$

The lower inhomogeneous equation arises when  $\vec{x}'$  is inside the sample and the upper homogeneous one otherwise (extinction equation). Furthermore, analogous homogeneous equations are obtained if the Green's function is replaced by auxiliary functions satisfying the same equations inside the sample, but without sources and without regard to boundary conditions. Thus one obtains the following integral equations associated with the interior of the sample:

$$\int_S d\vec{S} \cdot \{ \phi_i^{-\omega}(\vec{x}) \vec{b}^\omega(\vec{x}) - \phi^\omega(\vec{x}) \vec{b}_i^{-\omega}(\vec{x}) \} = 0, \quad (\text{A7})$$

with  $\phi_i, \vec{b}_i$  representing inside auxiliary functions.

## APPENDIX B: CONTINUOUS AND DISCRETE SINE AND COSINE FOURIER TRANSFORMS

The continuous cosine and sine transforms of even,  $E(x)$ , and odd,  $O(x)$ , functions are defined as

$$E_c(q) = \int_{-\infty}^{\infty} dx \cos(qx) E(x) = 2 \int_0^{\infty} dx \cos(qx) E(x), \quad (\text{B1})$$

$$O_s(q) = \int_{-\infty}^{\infty} dx \sin(qx) O(x) = 2 \int_0^{\infty} dx \sin(qx) O(x). \quad (\text{B2})$$

From these equations, it follows that  $E_c(-q) = E_c(q)$  and  $O_s(-q) = -O_s(q)$ . These may be inverted as follows:

$$E(x) = \frac{1}{2\pi} \int_{-\infty}^{\infty} dq \cos(qx) E_c(q) = \frac{1}{\pi} \int_0^{\infty} dq \cos(qx) E_c(q), \quad (\text{B3})$$

$$O(x) = \frac{1}{2\pi} \int_{-\infty}^{\infty} dq \sin(qx) O_s(q) = \frac{1}{\pi} \int_0^{\infty} dq \sin(qx) O_s(q). \quad (\text{B4})$$

A connection of these mentioned continuous sine and cosine Fourier transforms of Eqs. (B1)–(B4) with the usual discrete sine and cosine transforms is the following:

$$\begin{aligned} \frac{1}{2} E_c(q_k) &= \int_0^{\infty} dx \cos(q_k x) E(x) = \Delta E_k \\ &= \Delta \left\{ \frac{1}{2} [E_0 + E_N (-1)^k] + \sum_{j=1}^{N-1} \cos(q_k j \Delta) E_j \right\}, \end{aligned} \quad (\text{B5})$$

$$\begin{aligned} \frac{1}{2} O_s(q_k) &= \int_0^{\infty} dx \sin(q_k x) O(x) = \Delta O_k \\ &= \Delta \sum_{j=1}^{N-1} \sin(q_k j \Delta) O_j, \end{aligned} \quad (\text{B6})$$

where the points located between  $0 < x < L$  are discretized as follows:  $x_j = j\Delta$ ,  $j = 0, \dots, N$ , with  $L = N\Delta$ . Also,  $q_k = \pi k / N\Delta = \pi k / L$ .

Following the continuous formulas, the inverse discrete cosine and sine transforms are the following:

$$\begin{aligned} E(x_j) &= E_j = \frac{1}{\pi} \int_0^{\infty} dq \cos(qx_j) E_c(q) \\ &= \frac{2}{N} \left\{ \frac{1}{2} [E_{k=0} + E_{k=N} (-1)^j] + \sum_{k=1}^{N-1} \cos(q_k j \Delta) E_k \right\}, \end{aligned} \quad (\text{B7})$$

$$O(x_j) = \frac{1}{\pi} \int_0^{\infty} dq \sin(qx_j) O_s(q) = \frac{2}{N} \sum_{k=1}^{N-1} \sin(q_k j \Delta) O_k, \quad (\text{B8})$$

with  $q_k j \Delta = \pi k j / N$ .

## APPENDIX C: EVEN OBSTACLES AND THIN FILMS

By writing the fields in terms of even and odd functions with respect to  $x = 0$ , the extinction Eqs. (20) lead to  $[B(x) = B_e(x) + B_o(x), \Phi(x) = \Phi_e(x) + \Phi_o(x)]$

$$0 = \int_{-\infty}^{\infty} dx e^{-|k|\eta(x)} \{ \cos(kx) B_e''(x) + [k \sin(kx) \eta'(x) - |k| \cos(kx)] \Phi_e''(x) - i \sin(kx) B_o''(x) + i [k \cos(kx) \eta'(x) + |k| \sin(kx)] \Phi_o''(x) \}, \quad (C1)$$

$$0 = \int_{-\infty}^{\infty} dx e^{|k|\xi(x)} \{ \cos(kx) B_e^d(x) - [k \sin(kx) \xi'(x) + |k| \cos(kx)] \Phi_e^d(x) - i \sin(kx) B_o^d(x) - i [k \cos(kx) \xi'(x) - |k| \sin(kx)] \Phi_o^d(x) \}, \quad (C2)$$

$$0 = \int_{-\infty}^{\infty} dx e^{\pm |k| [l + \eta(x)]} \{ \cos(kx) B_e''(x) - i \sin(kx) B_o''(x) + [\cos(kx) (vk \pm \mu |k|) + \sin(kx) \eta'(x) (\mu k \pm v |k|)] \Phi_e''(x) - i [\sin(kx) (vk \pm \mu |k|) - \cos(kx) \eta'(x) (\mu k \pm v |k|)] \Phi_o''(x) \} + \int_{-\infty}^{\infty} dx e^{\pm |k| [-l + \xi(x)]} \{ \cos(kx) B_e^d(x) - i \sin(kx) B_o^d(x) - [\cos(kx) (vk \pm \mu |k|) + \sin(kx) \xi'(x) (\mu k \pm v |k|)] \Phi_e^d(x) + i [\sin(kx) (vk \pm \mu |k|) - \cos(kx) \xi'(x) (\mu k \pm v |k|)] \Phi_o^d(x) \}. \quad (C3)$$

Using the representation of the unknown fields in terms of inverse sine and cosine Fourier transforms (see next Appendix section B) leads to

$$0 = B_e''(k) - |k| \Phi_e''(k) - is(k) B_o''(k) + ik \Phi_o''(k) + \frac{1}{\pi} \int_0^{\infty} dq \{ C_u^{-|k|}(k, q) B_e''(q) - q S_u^{-|k|}(k, q) \Phi_e''(q) \} - \frac{i}{\pi} \int_0^{\infty} dq \{ s(k) S_u^{-|k|}(k, q) B_o''(q) - qs(k) C_u^{-|k|}(k, q) \Phi_o''(q) \}, \quad (C4)$$

$$0 = B_e^d(k) - |k| \Phi_e^d(k) - is(k) B_o^d(k) + ik \Phi_o^d(k) + \frac{1}{\pi} \int_0^{\infty} dq \{ C_d^{|k|}(k, q) B_e^d(q) - q S_d^{|k|}(k, q) \Phi_e^d(q) \} - \frac{i}{\pi} \int_0^{\infty} dq \{ s(k) S_d^{|k|}(k, q) B_o^d(q) - qs(k) C_d^{|k|}(k, q) \Phi_o^d(q) \}, \quad (C5)$$

$$0 = e^{\pm |k|l} \{ B_e''(k) - is(k) B_o''(k) + (kv \pm |k|\mu) [\Phi_e''(k) - is(k) \Phi_o''(k)] \} + \frac{e^{\pm |k|l}}{\pi} \int_0^{\infty} dq \{ C_u^{\pm |k|}(k, q) B_e''(q) - is(k) S_u^{\pm |k|}(k, q) B_o''(q) + q [v \pm s(k)\mu] [s(k) S_u^{\pm |k|}(k, q) \Phi_e''(q) - i C_u^{\pm |k|}(k, q) \Phi_o''(q)] \} + e^{\mp |k|l} \{ B_e^d(k) - is(k) B_o^d(k) - (kv \pm |k|\mu) [\Phi_e^d(k) - is(k) \Phi_o^d(k)] \} + \frac{e^{\mp |k|l}}{\pi} \int_0^{\infty} dq \{ C_d^{\pm |k|}(k, q) B_e^d(q) - is(k) S_d^{\pm |k|}(k, q) B_o^d(q) - q [v \pm s(k)\mu] [s(k) S_d^{\pm |k|}(k, q) \Phi_e^d(q) - i C_d^{\pm |k|}(k, q) \Phi_o^d(q)] \}. \quad (C6)$$

Indeed, the following equations help to understand the previous Eqs. (C4)–(C6):

$$f_{\eta}^{\pm}(x) \equiv e^{\pm |k|\eta(x)} [k \sin(kx) \eta' \pm |k| \cos(kx)] = \pm s(k) \frac{\partial}{\partial x} [\sin(kx) e^{\pm |k|\eta(x)}]. \quad (C7)$$

Then,

$$\int_{-\infty}^{\infty} dx \cos(qx) f_{\eta}^{\pm}(x) = \pm qs(k) \{ \pi [\delta(k - q) - \delta(k + q)] + S_u^{\pm |k|}(k, q) \}. \quad (C8)$$

Similarly,

$$\int_{-\infty}^{\infty} \cos(qx) f_{\xi}^{\pm}(x) = \pm qs(k) \{ \pi [\delta(k - q) - \delta(k + q)] + S_d^{\pm |k|}(k, q) \}. \quad (C9)$$

Notice that

$$[\cos(kx) (vk \pm \mu |k|) + \sin(kx) \eta'(x) (\mu k \pm v |k|)] = [\mu \pm s(k)v] [k \sin(kx) \eta'(x) \pm |k| \cos(kx)] \quad (C10)$$

and it leads through Eq. (C8) to

$$\int_{-\infty}^{\infty} dx \cos(qx) e^{\pm|k|\eta(x)} [\cos(kx)(vk \pm \mu|k|) + \sin(kx)\eta'(x)(\mu k \pm \nu|k|)] = q[v \pm s(k)\mu] \{ \pi [\delta(k-q) - \delta(k+q)] + S_u^{\pm|k|}(k, q) \}. \quad (\text{C11})$$

Also,

$$\begin{aligned} g_{\eta}^{\pm}(x) &\equiv e^{\pm|k|\eta(x)} [k \cos(kx)\eta' \mp |k| \sin(kx)] \\ &= \pm s(k) \frac{\partial}{\partial x} [\cos(kx) e^{\pm|k|\eta(x)}]. \end{aligned} \quad (\text{C12})$$

Then,

$$\int_{-\infty}^{\infty} dx \sin(qx) g_{\eta}^{\pm}(x) = \mp qs(k) \{ \pi [\delta(k-q) + \delta(k+q)] + C_u^{\pm|k|}(k, q) \}. \quad (\text{C13})$$

Also,

$$[\sin(kx)(vk \pm \mu|k|) - \cos(kx)\eta'(x)(\mu k \pm \nu|k|)] = -[\mu \pm s(k)\nu] [k \cos(kx)\eta'(x) \mp |k| \sin(kx)] \quad (\text{C14})$$

and it leads through Eq. (C13) to

$$\int_{-\infty}^{\infty} dx e^{\pm|k|\eta(x)} \sin(qx) [\sin(kx)(vk \pm \mu|k|) - \cos(kx)\eta'(x)(\mu k \pm \nu|k|)] = q[v \pm \mu s(k)] \{ \pi [\delta(k-q) + \delta(k+q)] + C_u^{\pm|k|}(k, q) \}. \quad (\text{C15})$$

#### APPENDIX D: SEMI-INFINITE MEDIUM

We consider that the semi-infinite magnetized medium is located in  $y \geq 0$  and that the geometric perturbation of the lower surface ( $y \simeq 0$ ) is  $\xi(x) = -\eta(x)$ , i.e.,  $y(x) = -\eta(x)$  represents the perturbed surface. One may obtain extinction equations for semi-infinite mediums as special cases of the extinction equations (24) and (25):

$$0 = B_e(k) - is(k)B_o(k) - H_e(k) + is(k)H_o(k) + \frac{2}{N} \sum_q \{ C_-(k, q)[B_e(q) + is(k)H_o(q)] - S_-(k, q)[H_e(q) + is(k)B_o(q)] \}, \quad (\text{D1})$$

$$\begin{aligned} 0 &= [s(k)\Omega - h][B_e(k) - is(k)B_o(k)] - [h - s(k)\Omega + 1][H_e(k) - is(k)H_o(k)] + \frac{2}{N} \sum_q \{ [s(k)\Omega - h][C_+(k, q)B_e(q) \\ &\quad - is(k)S_+(k, q)B_o(q)] - [h - s(k)\Omega + 1][S_+(k, q)H_e(q) - is(k)C_+(k, q)H_o(q)] \}, \end{aligned} \quad (\text{D2})$$

with

$$\begin{aligned} C_{\pm}(k, q) &\equiv \int_{-\infty}^{\infty} dx \cos(qx) \cos(kx) (e^{\pm|k|\eta(x)} - 1), \\ S_{\pm}(k, q) &\equiv s(k) \int_{-\infty}^{\infty} dx \sin(qx) \sin(kx) (e^{\pm|k|\eta(x)} - 1). \end{aligned} \quad (\text{D3})$$

Considering the cases  $s(k) = \text{sgn}(k) = \pm 1$ , one gets four extinction equations from Eqs. (D1) and (D2):

$$0 = B_e(k) - iB_o(k) - H_e(k) + iH_o(k) + \frac{2}{N} \sum_q \{ C_-(k, q)[B_e(q) + iH_o(q)] - S_-(k, q)[H_e(q) + iB_o(q)] \}, \quad (\text{D4})$$

$$0 = B_e(k) + iB_o(k) - H_e(k) - iH_o(k) + \frac{2}{N} \sum_q \{ C_-(k, q)[B_e(q) - iH_o(q)] - S_-(k, q)[H_e(q) - iB_o(q)] \}, \quad (\text{D5})$$

$$\begin{aligned} 0 &= (\Omega - h)[B_e(k) - iB_o(k)] - (h - \Omega + 1)[H_e(k) - iH_o(k)] + \frac{2}{N} \sum_q \{ (\Omega - h)[C_+(k, q)B_e(q) \\ &\quad - iS_+(k, q)B_o(q)] - (h - \Omega + 1)[S_+(k, q)H_e(q) - iC_+(k, q)H_o(q)] \}, \end{aligned} \quad (\text{D6})$$

$$\begin{aligned} 0 &= (\Omega + h)[B_e(k) + iB_o(k)] + (h + \Omega + 1)[H_e(k) + iH_o(k)] + \frac{2}{N} \sum_q \{ (\Omega + h)[C_+(k, q)B_e(q) \\ &\quad + iS_+(k, q)B_o(q)] + (h + \Omega + 1)[S_+(k, q)H_e(q) + iC_+(k, q)H_o(q)] \}. \end{aligned} \quad (\text{D7})$$

By defining new variables

$$U_{\pm} \equiv B_e \pm iH_o, \quad V_{\pm} \equiv H_e \pm iB_o \quad (\text{D8})$$

and using the matrices  $P_{\pm}, R_{\pm}$  defined in Eqs. (27), Eqs. (D4)–(D7) become

$$0 = P_- U_+ - R_- V_+, \quad (\text{D9})$$

$$0 = P_- U_- - R_- V_-, \quad (\text{D10})$$

$$0 = (\Omega - h - 1/2)(P_+ U_- + R_+ V_-) - R_+ V_+/2 + P_+ U_+/2, \quad (\text{D11})$$

$$0 = (\Omega + h + 1/2)(P_+ U_+ + R_+ V_+) + R_+ V_-/2 - P_+ U_-/2. \quad (\text{D12})$$

In the case of no geometric defects these equations become  $U_+ = V_+, U_- = V_-$ , and

$$0 = (\Omega - h - 1/2)U_-, \quad (\text{D13})$$

$$0 = (\Omega + h + 1/2)U_+. \quad (\text{D14})$$

The modes resulting from Eq. (D13) correspond to surface modes of positive frequency  $\Omega = h + 1/2$ , with  $U_-(k) = V_-(k) \neq 0$ ,  $U_+(k) = V_+(k) = 0$ . The latter [using Eqs. (D8)] leads to  $B_e = -iH_o, H_e = -iB_o$ , and together with  $U_- = V_-$  leads to  $H_o = iH_e, B_o = iB_e$ . The last equality leads to

$$B(x) = (2/N)[B_e \cos(kx) + B_o \sin(kx)] = (2/N)B_e e^{ikx}, \quad (\text{D15})$$

meaning that there is only propagation to the right on the semi-infinite surface, as announced [here  $k > 0$  and the time dependence is  $\exp(-i\omega t)$ ].

By using the following matrices:  $T \equiv P_-^{-1}R_-, S \equiv P_+T + R_+$ , and  $Q \equiv P_+T - R_+$ , the system of Eqs. (D9)–(D12) becomes a regular eigenvalue ( $\Omega$ ) problem:

$$0 = \begin{pmatrix} (h + 1/2)I - \Omega I & -QS^{-1}/2 \\ QS^{-1}/2 & -(h + 1/2)I - \Omega I \end{pmatrix} \begin{pmatrix} SV_- \\ SV_+ \end{pmatrix}. \quad (\text{D16})$$

A final step leads to

$$0 = \left( [(h + 1/2)^2 - \Omega^2]I \quad -(QS^{-1})^2/4 \right) (SV_+). \quad (\text{D17})$$

Thus the eigenvalues  $\Omega^2$  are equal to the eigenvalues of the matrix  $-(QS^{-1})^2/4$  plus  $(h + 1/2)^2$ .

#### APPENDIX E: CASE OF THIN FILM WITH FLAT SURFACES

The spin wave modes of a film with flat surfaces may be solved by the standard method, i.e., by solving the magnetostatic Maxwell equations subject to boundary conditions, and the Landau Lifshitz equations (see discussion in Sec. II B). The plane wave solution for the magnetostatic potential is of the form

$$\phi(x, y, t) = e^{i(kx - \omega t)} \phi(y), \quad (\text{E1})$$

with  $\phi(y)$  given by

$$\begin{aligned} \phi_u(y) &= U e^{-|k|(y-l)}, & y > l, \\ \phi_i(y) &= I_+ e^{|k|y} + I_- e^{-|k|y}, & -l < y < l, \\ \phi_d(y) &= D e^{|k|(y+l)}, & y < -l. \end{aligned} \quad (\text{E2})$$

Notice that the profile  $f(y)$  of the magnetostatic plane wave of Eqs. (62) corresponds to  $\phi(y)$  evaluated for  $s = \text{sgn}(k) > 0$ . Applying the boundary conditions of continuous magnetostatic potential and  $y$  component of the magnetic induction

$b_y$  at the surfaces  $y = \pm l$  of the film, one obtains

$$0 = \begin{pmatrix} (\mu + 1 + sv)e^{|k|l} & (-\mu + 1 + sv)e^{-|k|l} \\ (\mu - 1 + sv)e^{-|k|l} & (-\mu - 1 + sv)e^{|k|l} \end{pmatrix} \begin{pmatrix} I_+ \\ I_- \end{pmatrix}, \quad (\text{E3})$$

which is equivalent to

$$0 = \begin{pmatrix} \left(2 + \frac{1}{h+s\Omega}\right)e^{|k|l} & -\frac{1}{h-s\Omega}e^{-|k|l} \\ \frac{1}{h+s\Omega}e^{-|k|l} & -(2 + \frac{1}{h-s\Omega})e^{|k|l} \end{pmatrix} \begin{pmatrix} I_+ \\ I_- \end{pmatrix}. \quad (\text{E4})$$

Imposing the determinant of the previous matrix to be null leads to the frequencies of the DE surface modes of Eq. (1) (there are solutions with equivalent negative frequencies). From the eigenvector associated with Eq. (E4) at positive frequency (fixed value of  $k$ ) one deduces that the ratio of the potentials evaluated at the surfaces is

$$\frac{\phi(l)}{\phi(-l)} = \frac{U}{D} = \sqrt{\frac{h + 1/2 - s\Omega}{h + 1/2 + s\Omega}}, \quad (\text{E5})$$

which shows that the amplitude of the spin wave in propagation to the right ( $\Omega > 0$  and  $k > 0$ ) is significant in the lower

surface and vice versa for propagation to the left, i.e., in that case significant in the upper surface.

In the case of a film with flat surfaces one may also obtain the antisymmetric and symmetric modes of Eqs. (93) and (94) through our extinction equations. Indeed, Eqs. (39)–(42) for the antisymmetric modes become effectively  $B_e^a = H_e^a$ ,  $B_o^s = H_o^s$ , and

$$\begin{aligned} 0 &= -2\Omega D_+ H_o^s - i[(2h+1)D_+ + D_-]H_e^a, \\ 0 &= i[(2h+1)D_+ - D_-]H_o^s - 2\Omega D_+ H_e^a. \end{aligned} \quad (\text{E6})$$

These equations may be written in matrix form as

$$0 = \begin{pmatrix} -\Omega I & -i[(h + \frac{1}{2})I + \frac{D_-^2}{2}] \\ i[(h + \frac{1}{2})I - \frac{D_-^2}{2}] & -\Omega I \end{pmatrix} \begin{pmatrix} D_+ H_o^s \\ D_+ H_e^a \end{pmatrix}. \quad (\text{E7})$$

Imposing the determinant of the previous equations to be null leads to the dispersion relation of Damon Eshbach (DE) modes. For the positive frequencies (there are  $\pm$  pairs of solutions), the eigenvector corresponds to

$$\frac{iH_o^s(k)}{H_e^a(k)} = \sqrt{\frac{h + 1/2 + e^{-2|k|l}/2}{h + 1/2 - e^{-2|k|l}/2}}. \quad (\text{E8})$$

Also, Eqs. (53)–(56) for the symmetric modes become effectively  $B_e^s = H_e^s$ ,  $B_o^a = H_o^a$ , and

$$\begin{aligned} 0 &= -2\Omega D_+ H_o^a - i[(2h+1)D_+ - D_-]H_e^s, \\ 0 &= i[(2h+1)D_+ + D_-]H_o^a - 2\Omega D_+ H_e^s. \end{aligned} \quad (\text{E9})$$

These equations may be written in matrix form as

$$0 = \begin{pmatrix} -\Omega I & -i[(h + \frac{1}{2})I - \frac{D_-^2}{2}] \\ i[(h + \frac{1}{2})I + \frac{D_-^2}{2}] & -\Omega I \end{pmatrix} \begin{pmatrix} D_+ H_o^a \\ D_+ H_e^s \end{pmatrix}. \quad (\text{E10})$$

Imposing the determinant of the previous equations to be null leads again to the frequency eigenvalues of the DE modes of Eq. (1). For the positive frequencies, the eigenvector corresponds to

$$\frac{iH_o^a(k)}{H_e^s(k)} = \sqrt{\frac{h + 1/2 - e^{-2|k|l}/2}{h + 1/2 + e^{-2|k|l}/2}}. \quad (\text{E11})$$

The results for the eigenvectors of the antisymmetric and symmetric modes of Eqs. (E8) and (E11) may be verified by use of the “standard” solution of Eq. (E2) and indeed more directly by use of Eq. (E5).

- 
- [1] V. V. Kruglyak, S. O. Demokritov, and D. Grundler, *Magnonics*, *J. Phys. D* **43**, 264001 (2010).
- [2] A. V. Chumak, V. I. Vasyuchka, A. A. Serga, and B. Hillebrands, *Magnon spintronics*, *Nat. Phys.* **11**, 453 (2015).
- [3] A. I. Akhiezer, V. G. Bariakhtar, V. G. Barjachtar, and S. V. Peletminskiĭ, *Spin Waves*, North-Holland Series in Low Temperature Physics (North-Holland Publishing Company, Amsterdam, 1968).
- [4] A. G. Gurevich and G. A. Melkov, *Magnetization Oscillations and Waves* (CRC Press, Boca Raton, FL, 1996).
- [5] S. O. Demokritov and A. N. Slavin, *Magnonics. From Fundamentals to Applications*, Topics in Applied Physics (Springer, Berlin, 2013).
- [6] B. Diény *et al.*, Opportunities and challenges for spintronics in the microelectronics industry, *Nat. Electron.* **3**, 446 (2020).
- [7] A. Barman *et al.*, The 2021 Magnonics Roadmap, *J. Phys.: Condens. Matter* **33**, 413001 (2021).
- [8] J. R. Eshbach and R. W. Damon, Surface magnetostatic modes and surface spin waves, *Phys. Rev.* **118**, 1208 (1960).
- [9] M. J. Hurben and C. E. Patton, Theory of magnetostatic waves for in-plane magnetized isotropic films, *J. Magn. Magn. Mater.* **139**, 263 (1995).
- [10] E. O. Kamenetskii, Self-induced quasistationary magnetic fields, *Phys. Rev. E* **73**, 016602 (2006).
- [11] O. Büttner, M. Bauer, S. O. Demokritov, B. Hillebrands, Y. S. Kivshar, V. Grimalsky, Y. Rapoport, and A. N. Slavin, Linear and nonlinear diffraction of dipolar spin waves in yttrium iron garnet films observed by space- and time-resolved Brillouin light scattering, *Phys. Rev. B* **61**, 11576 (2000).
- [12] M. Bailleul, D. Olligs, C. Fermon, and S. O. Demokritov, Spin waves propagation and confinement in conducting films at the micrometer scale, *Europhys. Lett.* **56**, 741 (2001).
- [13] J. Förster, S. Wintz, J. Bailey, S. Finizio, E. Josten, C. Dubs, D. A. Bozhko, H. Stoll, G. Dieterle, N. Träger, J. Raabe, A. N. Slavin, M. Weigand, J. Gräfe, and G. Schütz, Nanoscale X-ray imaging of spin dynamics in yttrium iron garnet, *J. Appl. Phys.* **126**, 173909 (2019).
- [14] C. S. Chang, M. Kostylev, E. Ivanov, J. Ding, and A. O. Adeyeye, The phase accumulation and antenna near field of microscopic propagating spin wave devices, *Appl. Phys. Lett.* **104**, 032408 (2014).
- [15] S. O. Demokritov, A. A. Serga, A. André, V. E. Demidov, M. P. Kostylev, B. Hillebrands, and A. N. Slavin, Tunneling of dipolar spin waves through a region of inhomogeneous magnetic field, *Phys. Rev. Lett.* **93**, 047201 (2004).
- [16] M. P. Kostylev, A. A. Serga, T. Schneider, T. Neumann, B. Leven, B. Hillebrands, and R. L. Stamps, Resonant and nonresonant scattering of dipole-dominated spin waves from a region of inhomogeneous magnetic field in a ferromagnetic film, *Phys. Rev. B* **76**, 184419 (2007).
- [17] D. R. Birt, B. O’Gorman, M. Tsoi, X. Li, V. E. Demidov, and S. O. Demokritov, Diffraction of spin waves from a submicrometer-size defect in a waveguide, *Appl. Phys. Lett.* **95**, 122510 (2009).
- [18] O. Nafa, B. Bourahla, and A. Khater, Scattering properties induced by an asymmetric nanowell on ferromagnetic ultrathin film, *J. Phys. Chem. Solids* **74**, 395 (2013).
- [19] O. V. Dobrovolskiy, R. Sachser, S. A. Bunyaev, D. Navas, V. M. Bevez, M. Zelent, W. Śmigaj, J. Rychły, M. Krawczyk, R. V. Vovk, M. Huth, and G. N. Kakazei, Spin-wave phase inverter upon a single nanodefekt, *ACS Appl. Mater. Interfaces* **11**, 17654 (2019).

- [20] A. Balaji, M. Kostylev, and M. Bailleul, Scattering of a magnetostatic surface spin wave from a one-dimensional step potential in a ferromagnetic film, *J. Appl. Phys.* **125**, 163903 (2019).
- [21] J. Iwasaki, A. J. Beekman, and N. Nagaosa, Theory of magnon-skyrmion scattering in chiral magnets, *Phys. Rev. B* **89**, 064412 (2014).
- [22] C. Schütte and M. Garst, Magnon-skyrmion scattering in chiral magnets, *Phys. Rev. B* **90**, 094423 (2014).
- [23] Z. Wang, H. Y. Yuan, Y. Cao, Z. X. Li, R. A. Duine, and P. Yan, Magnonic frequency comb through nonlinear magnon-skyrmion scattering, *Phys. Rev. Lett.* **127**, 037202 (2021).
- [24] J. Lan and J. Xiao, Skew scattering and side jump of spin wave across magnetic texture, *Phys. Rev. B* **103**, 054428 (2021).
- [25] V. Laliena, A. Athanasopoulos, and J. Campo, Scattering of spin waves by a Bloch domain wall: Effect of the dipolar interaction, *Phys. Rev. B* **105**, 214429 (2022).
- [26] K. A. Kotas, M. Moalic, M. Zelent, M. Krawczyk, and P. Gruszecki, Scattering of spin waves in a multimode waveguide under the influence of confined magnetic skyrmion, *APL Mater.* **10**, 091101 (2022).
- [27] R. Arias and D. L. Mills, Magnetostatic modes in ferromagnetic nanowires, *Phys. Rev. B* **70**, 094414 (2004).
- [28] R. Arias and D. L. Mills, Magnetostatic modes in ferromagnetic nanowires. II. A method for cross sections with very large aspect ratio, *Phys. Rev. B* **72**, 104418 (2005).
- [29] C. Jarufe and R. E. Arias, Magnonic and plasmonic band gaps in films with periodically modified surfaces, *Phys. Rev. B* **85**, 205411 (2012).
- [30] R. E. Arias, Spin-wave modes of ferromagnetic films, *Phys. Rev. B* **94**, 134408 (2016).
- [31] I. A. Armijo and R. E. Arias, Spin wave modes of multilayered ferromagnetic films, *Phys. Rev. B* **99**, 014432 (2019).
- [32] I. A. Armijo and R. E. Arias, Surface properties of ferromagnetic films and spin wave modes, *Phys. Rev. B* **107**, 214408 (2023).
- [33] J. H. Eberly, Quantum scattering theory in one dimension, *Am. J. Phys.* **33**, 771 (1965).
- [34] J. Formanek, On phase shift analysis of one-dimensional scattering, *Am. J. Phys.* **44**, 778 (1976).
- [35] D. W. L. Sprung, H. Wu, and J. Martorell, Poles, bound states, and resonances illustrated by the square well potential, *Am. J. Phys.* **64**, 136 (1996).
- [36] K. Y. Bliokh, V. D. Freilikher, and N. M. Makarov, Scattering by one-dimensional smooth potentials: Between wkb and born approximation, *Physica E* **27**, 262 (2005).
- [37] L. J. Boya, Quantum-mechanical scattering in one dimension, *Riv. Nuovo Cimento* **31**, 75 (2008).
- [38] S. S. Gupta and N. C. Srivastava, Power flow and energy distribution of magnetostatic bulk waves—in dielectric-layered structure, *J. Appl. Phys.* **50**, 6697 (1979).
- [39] F. Toigo, A. Marvin, V. Celli, and N. R. Hill, Optical properties of rough surfaces: General theory and the small roughness limit, *Phys. Rev. B* **15**, 5618 (1977).
- [40] E. Manousakis, *Practical Quantum Mechanics*, Modern Tools and Applications, Oxford Graduate Texts (Oxford University Press, Oxford, 2016).
- [41] F. H. Stillinger and D. R. Herrick, Bound states in the continuum, *Phys. Rev. A* **11**, 446 (1975).